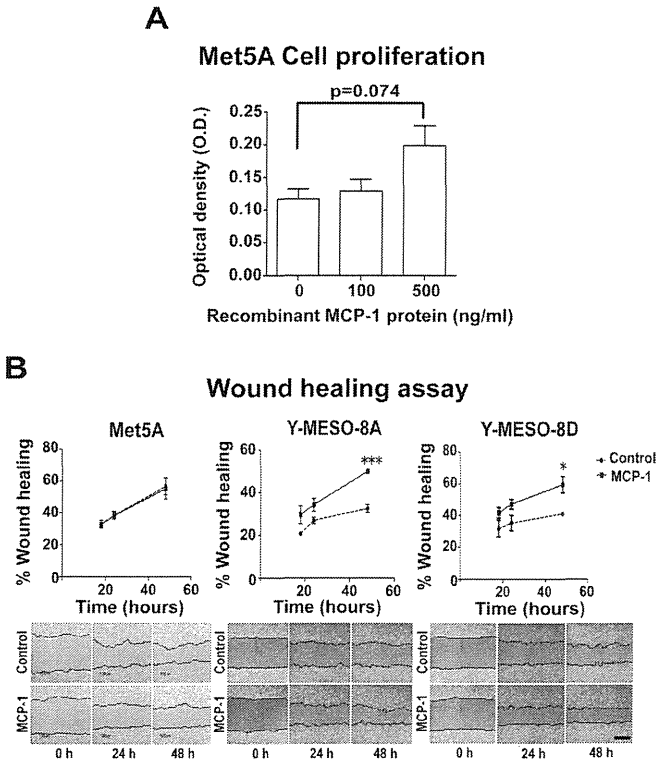

Fig. 5. Cancer-promoting effects of MCP-1. (**A**) Recombinant MCP-1 protein stimulates cell proliferation of the human mesothelial cell line MeT-5A, as measured by the MTT cell proliferation assay. (**B**) Recombinant MCP-1 protein induces the migration of the human mesothelioma cells Y-MESO-8A and Y-MESO-8D, as measured by the wound-healing assay. The results are shown as the mean ± SEM of three independent experiments. $^{*}P \leq 0.05$, $^{***}P \leq 0.001$.

a key molecule activated by asbestos fibers in mesothelial cells and macrophages that is responsible for inflammation. Our results suggested that asbestos fibers can cause a downregulation of adiponectin. The exact roles of leptin and PAI-1 in inflammation are still not entirely clear, although both were shown to be upregulated in obesity-related inflammation (43–45). A member of the prolactin superfamily, Prl2c5, was also upregulated. Current information regarding Prl2c5 is still relatively scarce, but this protein most probably shares many characteristics of prolactin, which is known to possess mitogenic property (46). Prolactin was newly found as an adipocytokine secreted by human adipose tissue (47,48). Several other genes more recently characterized as adipokines were also upregulated. Some of these genes, such as haptoglobin and lipocalin-2, bind to iron and can thus contribute to iron overload, which was shown to play an important role in asbestos-induced mesothelioma development (49). Another interesting upregulated peptide was secreted phosphoprotein 1, also known as osteopontin. Mesothelioma patients often have increased serum osteopontin levels and it was suggested to be a useful biomarker for the early diagnosis of mesothelioma (50). More detailed studies are needed to fully elucidate the potential pathogenic roles of these various dysregulated adipocytokines in mesothelial carcinogenesis. Moreover, a long-term study is needed to assess whether these alterations observed are long-term effects.

Interestingly, we found that chrysotile fibers appeared to be the most inflammogenic. Our results showed that chrysotile fibers dysregulated various adipocytokine levels to a higher extent than crocidolite and amosite fibers. This finding corroborates our recently published data that chrysotile fibers induced a significantly earlier development of malignant mesothelioma with intraperitoneal injection in rats compared with crocidolite and amosite fibers (49). The relatively stronger carcinogenicity of chrysotile fibers might be linked to a higher degree of adipose tissue inflammation. The reason underlying why chrysotile fibers seem to have a stronger inflammogenic effect on adipocytes is still not known, although our results showed that all types of asbestos fibers were internalized by the adipocytes.

To our knowledge, this is the first report of a potential association between dysregulated adipose endocrine function and asbestos-induced mesothelial carcinogenesis. We have shown that asbestos fibers are able to directly trigger an inflammatory response in adipocytes by dysregulating adipocytokine production. These adipocytokines might act locally to stimulate the growth/migration/survival of mesothelial cells and thus promote the development of malignant mesothelioma. The modulation of these adipocytokines might represent a novel strategy to extend the lifespan of mesothelioma patients.

Supplementary material

Supplementary Tables 1–3 and Figure 1 can be found at http://carcin.oxfordjournals.org/

Funding

Princess Takamatsu Cancer Research Fund (10-24213); Ministry of Health, Labour and Welfare of Japan (25-A-5); Ministry of Education, Culture, Sports, Science and Technology of Japan (24390094). The funders had no role in study design, data collection and analysis, decision to publish or preparation of the manuscript.

Conflict of Interest Statement: None declared.

References

1. Wagner,J.C. *et al.* (1960) Diffuse pleural mesothelioma and asbestos exposure in the North Western Cape Province. *Br. J. Ind. Med.*, **17**, 260–271.
2. Davies,P. *et al.* (1974) Asbestos induces selective release of lysosomal enzymes from mononuclear phagocytes. *Nature*, **251**, 423–425.
3. Hamilton,J.A. (1980) Macrophage stimulation and the inflammatory response to asbestos. *Environ. Health Perspect.*, **34**, 69–74.
4. Choe,N. *et al.* (1997) Pleural macrophage recruitment and activation in asbestos-induced pleural injury. *Environ. Health Perspect.*, **105** (suppl. 5), 1257–1260.
5. Ramos-Nino,M.E. *et al.* (2002) Mesothelial cell transformation requires increased AP-1 binding activity and ERK-dependent Fra-1 expression. *Cancer Res.*, **62**, 6065–6069.
6. Swain,W.A. *et al.* (2004) Activation of p38 MAP kinase by asbestos in rat mesothelial cells is mediated by oxidative stress. *Am. J. Physiol. Lung Cell. Mol. Physiol.*, **286**, L859–L865.
7. Yang,H. *et al.* (2006) TNF-alpha inhibits asbestos-induced cytotoxicity via a NF-kappaB-dependent pathway, a possible mechanism for asbestos-induced oncogenesis. *Proc. Natl Acad. Sci. USA*, **103**, 10397–10402.
8. Jagadeeswaran,R. *et al.* (2006) Functional analysis of c-Met/hepatocyte growth factor pathway in malignant pleural mesothelioma. *Cancer Res.*, **66**, 352–361.
9. Yang,H. *et al.* (2010) Programmed necrosis induced by asbestos in human mesothelial cells causes high-mobility group box 1 protein release and resultant inflammation. *Proc. Natl Acad. Sci. USA*, **107**, 12611–12616.
10. Whitaker,D. *et al.* (1984) Cytologic and tissue culture characteristics of asbestos-induced mesothelioma in rats. *Acta Cytol.*, **28**, 185–189.
11. Suzuki,Y. *et al.* (1984) Malignant mesothelioma induced by asbestos and zeolite in the mouse peritoneal cavity. *Environ. Res.*, **35**, 277–292.
12. Toyokuni,S. (2009) Mechanisms of asbestos-induced carcinogenesis. *Nagoya J. Med. Sci.*, **71**, 1–10.
13. Bolton,R.E. *et al.* (1982) Variations in the carcinogenicity of mineral fibres. *Ann. Occup. Hyg.*, **26**, 569–582.
14. Carthew,P. *et al.* (1992) Intrapleural administration of fibres induces mesothelioma in rats in the same relative order of hazard as occurs in man after exposure. *Hum. Exp. Toxicol.*, **11**, 530–534.
15. Fantuzzi,G. (2005) Adipose tissue, adipokines, and inflammation. *J. Allergy Clin. Immunol.*, **115**, 911–9; quiz 920.
16. Greenberg,A.S. *et al.* (2006) Obesity and the role of adipose tissue in inflammation and metabolism. *Am. J. Clin. Nutr.*, **83**, 461S–465S.
17. Itoh,M. *et al.* (2011) Adipose tissue remodeling as homeostatic inflammation. *Int. J. Inflam.*, **2011**, 720926.

18. Bianchini,F. *et al.* (2002) Overweight, obesity, and cancer risk. *Lancet Oncol.*, **3**, 565–574.
19. Calle,E.E. *et al.* (2003) Overweight, obesity, and mortality from cancer in a prospectively studied cohort of U.S. adults. *N. Engl. J. Med.*, **348**, 1625–1638.
20. Reeves,G.K. *et al.* Million Women Study Collaboration. (2007) Cancer incidence and mortality in relation to body mass index in the Million Women Study: cohort study. *BMJ*, **335**, 1134.
21. Renehan,A.G. *et al.* (2008) Body-mass index and incidence of cancer: a systematic review and meta-analysis of prospective observational studies. *Lancet*, **371**, 569–578.
22. Hotamisligil,G.S. *et al.* (1993) Adipose expression of tumor necrosis factor-alpha: direct role in obesity-linked insulin resistance. *Science*, **259**, 87–91.
23. Sartipy,P. *et al.* (2003) Monocyte chemoattractant protein 1 in obesity and insulin resistance. *Proc. Natl Acad. Sci. USA*, **100**, 7265–7270.
24. Kanda,H. *et al.* (2006) MCP-1 contributes to macrophage infiltration into adipose tissue, insulin resistance, and hepatic steatosis in obesity. *J. Clin. Invest.*, **116**, 1494–1505.
25. van Kruijsdijk,R.C. *et al.* (2009) Obesity and cancer: the role of dysfunctional adipose tissue. *Cancer Epidemiol. Biomarkers Prev.*, **18**, 2569–2578.
26. Cousin,B. *et al.* (1999) A role for preadipocytes as macrophage-like cells. *FASEB J.*, **13**, 305–312.
27. Villena,J.A. *et al.* (2001) Adipose tissues display differential phagocytic and microbicidal activities depending on their localization. *Int. J. Obes. Relat. Metab. Disord.*, **25**, 1275–1280.
28. Usami,N. *et al.* (2006) Establishment and characterization of four malignant pleural mesothelioma cell lines from Japanese patients. *Cancer Sci.*, **97**, 387–394.
29. Nagai,H. *et al.* (2011) Diameter and rigidity of multiwalled carbon nanotubes are critical factors in mesothelial injury and carcinogenesis. *Proc. Natl Acad. Sci. USA*, **108**, E1330–E1338.
30. Okby,N.T. *et al.* (2000) Liposarcoma of the pleural cavity: clinical and pathologic features of 4 cases with a review of the literature. *Arch. Pathol. Lab. Med.*, **124**, 699–703.
31. Shen,W. *et al.* (2003) Adipose tissue quantification by imaging methods: a proposed classification. *Obes. Res.*, **11**, 5–16.
32. Nasreen,N. *et al.* (2000) MCP-1 in pleural injury: CCR2 mediates haptotaxis of pleural mesothelial cells. *Am. J. Physiol. Lung Cell. Mol. Physiol.*, **278**, L591–L598.
33. Fuentes,M.E. *et al.* (1995) Controlled recruitment of monocytes and macrophages to specific organs through transgenic expression of monocyte chemoattractant protein-1. *J. Immunol.*, **155**, 5769–5776.
34. Gunn,M.D. *et al.* (1997) Monocyte chemoattractant protein-1 is sufficient for the chemotaxis of monocytes and lymphocytes in transgenic mice but requires an additional stimulus for inflammatory activation. *J. Immunol.*, **158**, 376–383.
35. Lu,B. *et al.* (1998) Abnormalities in monocyte recruitment and cytokine expression in monocyte chemoattractant protein 1-deficient mice. *J. Exp. Med.*, **187**, 601–608.
36. Wei,E.K. *et al.* (2005) Low plasma adiponectin levels and risk of colorectal cancer in men: a prospective study. *J. Natl Cancer Inst.*, **97**, 1688–1694.
37. Dal Maso,L. *et al.* (2004) Circulating adiponectin and endometrial cancer risk. *J. Clin. Endocrinol. Metab.*, **89**, 1160–1163.
38. Mantzoros,C. *et al.* (2004) Adiponectin and breast cancer risk. *J. Clin. Endocrinol. Metab.*, **89**, 1102–1107.
39. Ishikawa,M. *et al.* (2005) Plasma adiponectin and gastric cancer. *Clin. Cancer Res.*, **11** (2 Pt 1), 466–472.
40. Goktas,S. *et al.* (2005) Prostate cancer and adiponectin. *Urology*, **65**, 1168–1172.
41. Ajuwon,K.M. *et al.* (2005) Adiponectin inhibits LPS-induced NF-kappaB activation and IL-6 production and increases PPARgamma2 expression in adipocytes. *Am. J. Physiol. Regul. Integr. Comp. Physiol.*, **288**, R1220–R1225.
42. Wulster-Radcliffe,M.C. *et al.* (2004) Adiponectin differentially regulates cytokines in porcine macrophages. *Biochem. Biophys. Res. Commun.*, **316**, 924–929.
43. Auwerx,J. *et al.* (1988) Tissue-type plasminogen activator antigen and plasminogen activator inhibitor in diabetes mellitus. *Arteriosclerosis*, **8**, 68–72.
44. Juhan-Vague,I. *et al.* (1989) Increased plasminogen activator inhibitor activity in non insulin dependent diabetic patients–relationship with plasma insulin. *Thromb. Haemost.*, **61**, 370–373.
45. Hauner,H. (2005) Secretory factors from human adipose tissue and their functional role. *Proc. Nutr. Soc.*, **64**, 163–169.
46. Welsch,C.W. *et al.* (1977) Prolactin and murine mammary tumorigenesis: a review. *Cancer Res.*, **37**, 951–963.
47. Zinger,M. *et al.* (2003) Prolactin expression and secretion by human breast glandular and adipose tissue explants. *J. Clin. Endocrinol. Metab.*, **88**, 689–696.
48. Hugo,E.R. *et al.* (2008) Prolactin release by adipose explants, primary adipocytes, and LS14 adipocytes. *J. Clin. Endocrinol. Metab.*, **93**, 4006–4012.
49. Jiang,L. *et al.* (2012) Iron overload signature in chrysotile-induced malignant mesothelioma. *J. Pathol.*, **228**, 366–377.
50. Pass,H.I. *et al.* (2005) Asbestos exposure, pleural mesothelioma, and serum osteopontin levels. *N. Engl. J. Med.*, **353**, 1564–1573.

Received December 5, 2012; revised June 25, 2013; accepted July 31, 2013

Lung Cancer 83 (2014) 23–29

Contents lists available at ScienceDirect

Lung Cancer

journal homepage: www.elsevier.com/locate/lungcan

RASSF3 downregulation increases malignant phenotypes of non-small cell lung cancer

Asuki Fukatsu[a,d], Futoshi Ishiguro[a,e], Ichidai Tanaka[a,d], Takumi Kudo[g,h], Kentaro Nakagawa[g], Keiko Shinjo[a,b], Yutaka Kondo[a,c], Makiko Fujii[a], Yoshinori Hasegawa[d], Kenji Tomizawa[i], Tetsuya Mitsudomi[i,1], Hirotaka Osada[a,f], Yutaka Hata[g], Yoshitaka Sekido[a,f,*]

[a] Division of Molecular Oncology, Aichi Cancer Center Research Institute, 1-1 Kanokoden, Chikusa-ku, Nagoya 464-8681, Japan
[b] Division of Oncological Pathology, Aichi Cancer Center Research Institute, 1-1 Kanokoden, Chikusa-ku, Nagoya 464-8681, Japan
[c] Division of Epigenomics, Aichi Cancer Center Research Institute, 1-1 Kanokoden, Chikusa-ku, Nagoya 464-8681, Japan
[d] Department of Respiratory Medicine, Graduate School of Medicine, Nagoya University, Nagoya 466-8550, Japan
[e] Department of General Thoracic Surgery, Graduate School of Medicine, Nagoya University, Nagoya 466-8550, Japan
[f] Department of Cancer Genetics, Graduate School of Medicine, Nagoya University, Nagoya 466-8550, Japan
[g] Department of Medical Biochemistry, Graduate School of Medicine, Tokyo Medical and Dental University, Tokyo 113-8519, Japan
[h] Department of Neurosurgery, Graduate School of Medicine, Tokyo Medical and Dental University, Tokyo 113-8519, Japan
[i] Department of Thoracic Surgery, Aichi Cancer Center Hospital, 1-1 Kanokoden, Chikusa-ku, Nagoya 464-8681, Japan

ARTICLE INFO

Article history:
Received 12 February 2013
Received in revised form 5 September 2013
Accepted 21 October 2013

Keywords:
Non-small cell lung cancer
Lymph node metastasis
Pleural invasion
Tumor suppressor
RASSF3
EGFR

ABSTRACT

Background: Ras-Association Family1A (RASSF1A) is a well-established tumor suppressor. Ten RASSF homologues comprise this family, and each member is considered a tumor suppressor. RASSF3 is one of the RASSF family members, but its function has not yet been clarified. Recently, we found that RASSF3 interacts with MDM2 and facilitates its ubiquitination, which induces apoptosis through p53 stabilization. However, the role of RASSF3 in human malignancies remains largely unknown.
Patients and methods: Ninety-five non-small cell lung cancer (NSCLC) patients from Nagoya University Hospital and 45 NSCLC patients from Aichi Cancer Center Hospital underwent pulmonary resection at each hospital, and lung cancer and corresponding non-cancerous lung tissues were collected. The expression levels of *RASSF3* were analyzed using quantitative real-time reverse transcription PCR. We performed statistical analysis to investigate the correlation with *RASSF3* expression and the clinicopathological characteristics. We also transfected RASSF3-siRNA into NSCLC cells, and performed motility assays to evaluate the influence on migration ability.
Results: *RASSF3* expression levels were downregulated in 125 of a total 140 NSCLCs. In a multivariate logistic regression analysis, the low *RASSF3* expression group below the median value was independently correlated with progressive phenotypes (lymph node metastasis and pleural invasion), non-adenocarcinoma histology and wild-type epidermal growth factor receptor (EGFR) status. In motility assays, RASSF3-knockdown NSCLC cells increased the migration rate compared to the control cells.
Conclusions: We found that the expression levels of *RASSF3* were frequently downregulated in NSCLCs. Downregulation of *RASSF3* strongly correlated with the progressive phenotypes of NSCLCs and EGFR wild-type status. In vitro studies also suggested that *RASSF3* downregulation increases migration ability of lung cancer cells. Together, our findings indicate *RASSF3* is a candidate tumor suppressor gene of NSCLCs.

1. Introduction

Non-small cell lung cancer (NSCLC) is one of the most common human malignancies and its prognosis remains poor [1]. With the advance of molecular biology, various genetic/epigenetic alterations have been found to be associated with biological behaviors of human lung cancer cells.

Ten homologues, RASSF1 to RASSF10, comprise the RASSF family [2–5 review], which has drawn considerable attention over the

* Corresponding author at: Division of Molecular Oncology, Aichi Cancer Center Research Institute, 1-1 Kanokoden, Chikusa-ku, Nagoya 464-8681, Japan. Tel.: +81 52 764 2983; fax: +81 52 764 2993.
E-mail address: ysekido@aichi-cc.jp (Y. Sekido).
[1] Present address: Department of Thoracic Surgery, Kinki University Faculty of Medicine, 377-2 Ohno-Higashi, Osaka-Sayama 589-8511, Japan.

0169-5002/$ – see front matter © 2013 Elsevier Ireland Ltd. All rights reserved.
http://dx.doi.org/10.1016/j.lungcan.2013.10.014

last decade, because one member of this family, RASSF1A, is a well-established tumor suppressor [6,7]. *RASSF1A* has shown to be ubiquitously expressed in non-tumor lung tissues but frequently silenced in lung tumors due to CpG island methylation of its promoter [6–9]. The reexpression of *RASSF1A* in cancer cell lines led to suppress cell proliferation [6,7] and hypermethylation of the *RASSF1A* promoter region correlated with a poor prognosis and advanced stage of common malignancies [10–13].

RASSF1 to RASSF6 contains Ras-association (RA) domain in the C-terminus (C-terminal RASSF), whereas RASSF7 to RASSF10 have a RA domain in the N-terminus (N-terminal RASSF). Besides RASSF1A, other RASSF members have also been reported to be downregulated in several human cancers and considered as tumor suppressors. RASSF3, the smallest member of the C-terminal RASSF [14], was shown to be overexpressed in mammary gland of tumor-resistant mouse mammary tumor virus (MMTV)/neu mice compared to tumor-susceptible MMTV/neu littermates or non-transgenic mice [15]. Recently, we also found that exogenous RASSF3 directly interacts with MDM2 and facilitates its ubiquitination, which induces apoptosis through increasing p53 stability [16]. These data suggest that RASSF3 functions as a tumor suppressor like RASSF1A. However, the exact roles of RASSF3 in human malignancies and its clinicopathological features remain largely unknown. In this study, we found that the downregulation of RASSF3 expression was frequently observed in NSCLCs, which correlates with lymph node metastasis, pleural invasion, EGFR wild-type status and adenocarcinoma histology independently. We also found that the suppression of RASSF3 by siRNA in NSCLC cell lines increases cell motility.

2. Materials and methods

2.1. Clinical specimens

We studied two cohorts; 95 and 45 patients with NSCLC who underwent pulmonary resection at Nagoya University (NU) Hospital (March 2004–June 2006) and Aichi Cancer Center (ACC) Hospital (January 2006–December 2006), respectively. Characteristics of the patients at NU and ACC are listed in Supplementary Tables 1 and 2, respectively. The treatment policy was decided according to the standard protocol of each hospital, and fully informed written consent was obtained from all patients prior to tissue collection under ethical approval obtained at either hospital. Tumor samples from both hospitals and corresponding normal lung tissue samples (peripheral lung as distant from the cancerous lesions as possible) only from NU were snap frozen and stored at −80 °C.

2.2. RNA and DNA preparations and reverse transcription (RT)

Total RNA was extracted from tumor and non-tumor samples using an RNeasy Kit (Qiagen, Tokyo, Japan) according to the manufacturer's instructions. In NU cases, first strand cDNA was generated from a total RNA (1500 ng) extracted from grossly resected frozen tissues using SuperScript III (Invitrogen, Tokyo, Japan). In ACC cases, fresh tumor specimens were tapped on a slide glass, which left enriched tumor cells on the slide, and then total RNA was isolated, following first strand cDNA synthesis from a total RNA (2 ng) using High Capacity cDNA Reverse Transcription Kit (Applied Biosystems, Tokyo, Japan).

Genomic DNA was extracted using a QIAamp DNA Mini Kit (Qiagen) according to the manufacturer's instructions.

2.3. Statistical analysis

The clinicopathological characteristics of the patients were obtained from medical records. Overall survival (OS) and progression-free survival (PFS) was calculated from the date of pulmonary resection to the date of death and recurrence, respectively. Patients without the known date of death or recurrence were censored at the time of the last follow-up.

For comparisons of proportions, the χ^2 test was used. The Kaplan–Meier method was conducted to estimate the probability of survival as a function of time, and survival differences were analyzed using log-rank test. The logistic regression analysis was used to test for significant differences in *RASSF3* gene expression within multiple groups: such as age, sex, smoking history, TNM stage, size, lymph node metastasis, lymph and venous invasion, pleural invasion, and gene mutations. The level of significance was set at $p < 0.05$.

2.4. Wound healing assay

For wound healing assay, five cell lines (A549, HCC193, NCI-H23, VMRC-LCD, and BEAS-2B) were transfected with siRNA, re-plated to 3.5 cm dishes 48 h after transfection, and grown to confluence. The cells were damaged using 1–200 μl beveled orifice tip (Quality Scientific Plastics, San Diego, CA) and then allowed to migrate. Photographs were taken at the initial time, 12 and 24 h later. Three independent fields were recorded for each experiment. Migration rate was calculated as a − b/a (a and b represent the widths of the fissure at initial the time and each respective time point).

2.5. Transwell migration assay

The 3-dimension cell motility of five cell lines (A549, HCC193, NCI-H23, VMRC-LCD, and BEAS-2B) was measured with the transwell assay using a chamber containing the polyethylene terephthalate filter membrane with 8-μm pores (Falcon, Franklin Lakes, NJ). For each experiment, 48 h after siRNA transfection 1×10^5 transfected cells in 500 μl medium were seeded in the chamber, which was placed in 24-well plate containing 1 ml of RPMI1640 medium with 0.4% FCS. After incubation for 24 h, the chambers were fixed and stained using Diff Quick stain (Sysmex, Kobe, Japan). The numbers of migrated cells were counted using phase-contrast microscopy at ×200 magnifications in the three randomly selected fields.

2.6. Quantitative real-time RT-PCR

Quantitative real-time RT-PCR was performed on first strand cDNA using TaqMan probes and the TaqMan Gene Expression Master Mix (Applied Biosystems). TaqMan probes for *RASSF3* (Hs 00415584_m1) and *GAPDH* (Hs 03929097_g1) were purchased from Applied Biosystems and the amplification was performed on an ABI PRISM 7500 Fast real-time PCR system (Applied Biosystems). Quantification was performed in triplicate. The *RASSF3* expression was normalized with an internal control, *GAPDH* using Δ-ΔC_T method, and presented as a relative expression level using a ratio to the average of *RASSF3*/*GAPDH* of the mean of the 95 non-cancerous lung tissues, which was arbitrarily set at 1.

Additional materials and methods are described in the Supplementary Materials and Methods.

3. Results

3.1. RASSF3 expression significantly reduced in NSCLCs

To determine whether or not the *RASSF3* gene is involved in lung carcinogenesis, we first studied the *RASSF3* gene expression using 95 NSCLC samples with their corresponding normal lung tissue samples which we collected at Nagoya University (NU) Hospital (Fig. 1A and B). We found that most of the lung cancer tissues (87

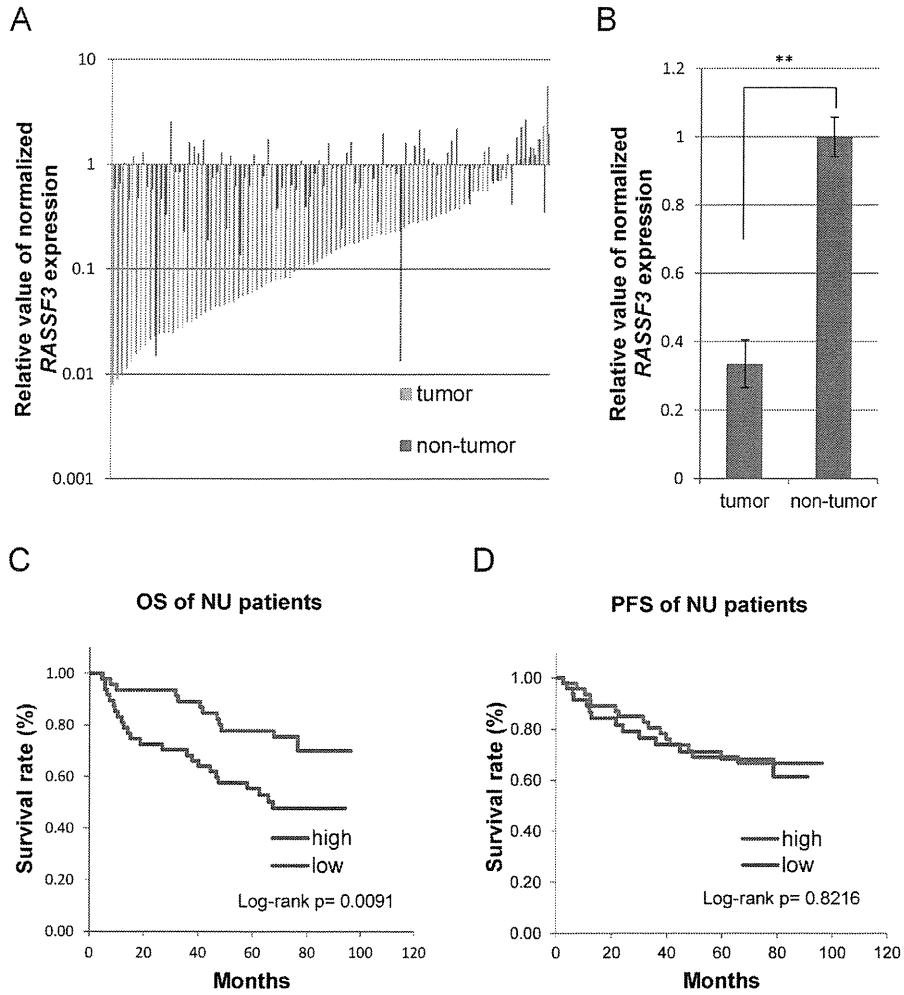

Fig. 1. (A) Relative expression levels of the *RASSF3* gene of NSCLC tumor samples from NU (Nagoya University) hospital and their corresponding non-cancerous lung tissues. Mean of *RASSF3* expression levels of the non-tumor samples was arbitrarily set as 1.0. Expression levels of tumor (blue line) and lung tissue (red line) are indicated side by side from the same patients, with the lowest *RASSF3* level of the tumor starting from the left. (B) Comparison of mean *RASSF3* expression levels between tumor and non-tumor samples. The reduction of *RASSF3* expression in tumor tissues was statistically significant. (C) and (D) Kaplan–Meier analysis of patients for overall survival (OS) (C) and progression-free survival (PFS) (D). The low *RASSF3* expression group showed a significantly worse prognosis in OS but not associated with PFS.

of 95) showed a more significantly reduced level of *RASSF3* (blue line in Fig. 1A) than that in the corresponding normal lung tissue (red line in Fig. 1A), indicating that *RASSF3* is frequently downregulated in NSCLCs. The mean of relative values of normalized *RASSF3* expression was also shown to be significantly lower in tumors than in normal lung tissues (Fig. 1B).

3.2. Low expression of RASSF3 significantly associated with invasive/metastatic character, non-adenocarcinoma histology, and EGFR wild-type status

To determine the possible effects of *RASSF3* downregulation on malignant phenotypes of NSCLCs, we divided 95 cases into two, low ($n=48$) and high ($n=47$) expression groups, respectively, by the median value (=0.14), and conducted statistical analyses for clinicopathological features based on the *RASSF3* expression status. The association status between *RASSF3* expression and clinicopathological parameters is summarized in Table 1. We found that the low *RASSF3* expression group was associated with disease progression in the patients, including TNM stage II/III ($p=0.0011$), tumor size (30 mm<) ($p=0.0123$), lymph node metastasis (pN1<) ($p=0.0008$) and pleural invasion ($p=0.0497$). Low *RASSF3* expression was significantly infrequent in the tumors with *EGFR* mutation ($p=0.0013$). The low *RASSF3* was also less frequently detected in the tumors from female ($p=0.0118$), adenocarcinoma ($p=0.0001$) and never/light smokers ($p=0.0282$), which were known to be the factors related with *EGFR* mutation [17–19]. There was no relation between *RASSF3* expression and *KRAS* mutation ($p=0.6927$).

Next, in order to reveal the crucial parameters for low *RASSF3* expression, we performed logistic regression analysis (Table 2). Univariate logistic regression analysis (Table 2, left column) indicated the same associations as the χ^2 test. In multivariate analysis (Table 2, right column), low *RASSF3* expression was found to be independently associated with non-adenocarcinoma histology, lymph node metastasis, pleural invasion and wild-type *EGFR*.

Among 95 patients, recurrence of the disease was observed in 29 patients, and 36 patients died during follow-up. The median length for OS and PFS of the patients were 71.5 and 65.9 months, respectively (Fig. 1C and D). Statistical analysis revealed that the low *RASSF3* expression group was significantly associated with worse prognosis in OS for the patients ($p=0.0091$, log-rank test) but not in PFS ($p=0.8216$, log-rank test). Since these survival data suggested possible discrepancies, we checked the major causes of death among the 36 patients. Primary lung cancer was the main cause of death in 21, but the remaining 6 patients died of other lung diseases (COPD and pneumonia which did not develop during cancer treatment), 3 of other neoplasms (pancreas cancer and leukemia), one of cerebrovascular accident, one

Table 1
Relationship between clinicopathological features and *RASSF3* gene expression of NSCLC patients from NU.

Variables		*n*	*RASSF3* expression (cutoff = 0.14)		
			Low	High	*p*-Value[a]
Age	≤65	38	19	19	
	>65	57	29	28	0.9332
Sex	Female	29	9	20	
	Male	66	39	27	0.0118*
Smoking history (pack-year)	≤20	36	13	23	
	>20	59	35	24	0.0282*
Histology	Adenocarcinoma	63	23	40	
	Non-adenocarcinoma	32	25	7	0.0001**
	Squamous cell carcinoma	29	23	6	
	Large cell carcinoma	1	0	1	
	Adenosquamous carcinoma	2	2	0	
TNM stage (UICC-7)	Stage I	57	21	36	
	Stage II/III	38	27	11	0.0011**
Tumor size (mm)	≤30	54	21	33	
	>30	40	26	14	0.0123*
Lymph node metastasis	pN0	68	27	41	
	pN1-3	27	21	6	0.0008**
Lymph invasion	–	63	30	33	
	+	32	18	14	0.4265
Venous invasion	–	78	40	38	
	+	16	8	8	0.9255
Pleural invasion	–	51	21	30	
	+	44	27	17	0.0497*
EGFR mutation	Mutant	28	7	21	
	Wild	67	41	26	0.0013**
KRAS mutation	Mutant	6	3	3	
	Wild	89	45	44	0.6927

Values with statistical significance were indicated with * ($p < 0.05$) or ** ($p < 0.01$). NSCLC: non-small cell lung cancer; NU: Nagoya University Hospital; OS: overall survival; PFS: progression-free survival.
[a] χ^2-test.

of renal failure, one of liver cirrhosis and 3 of unknown etiology. Thus, we reanalyzed the disease-specific survival (DSS), and found no significant association with DSS ($p = 0.4527$, log-rank test) (Supplemental Fig. S1). These data suggested that low *RASSF3* expression may not be a sufficient predictor for OS or PFS of NSCLC patients.

3.3. Association of low RASSF3 expression with clinicopathological parameters in the other NSCLC cohort

In order to confirm the results above, we analyzed the other set of NSCLC samples that we collected in Aichi Cancer Center (ACC) Hospital. We again found the frequent downregulation of *RASSF3* in the patients' samples (38 of 45) (Supplementary Fig. S2A). Like the NU sample set, we divided the 45 cases into two groups by median value (=0.35) as the low- ($n = 22$) and high-expression groups ($n = 23$) and compared these two groups. As we observed in NU samples, similar associations of *RASSF3* expression with disease progression and *EGFR* mutation were detected in ACC samples (Supplementary Table 3). Although there was no significant difference in tumor size in this cohort, we confirmed that the advanced TNM stage and lymph node metastasis were significantly associated with low *RASSF3* expression. No relation between *RASSF3* expression and *KRAS* mutation or *TP53* mutation was also found. In multivariate logistic regression analysis, we found similar tendencies between low *RASSF3* expression and clinicopathological parameters such as non-adenocarcinoma histology and lymph node metastasis (Supplementary Table 4). However, we did not detect any independent statistical significance, which was probably due to the smaller cohort sample.

Among 45 patients, 10 died during follow-up, with the OS median length of 95.5 months (Supplementary Fig. S2B). *RASSF3* expression levels were not significantly associated with OS ($p = 0.4270$, log-rank test).

Table 2
Univariate and multivariate logistic regression analyses of the association between low *RASSF3* gene expression and clinicopathological features of NU patients.

Variables	Univariate				Multivariate			
	Odds ratio	95% CI		*p*-Value[a]	Odds ratio	95% CI		*p*-Value[a]
Age (>65)	1.0357	0.4557	2.3539	0.9332				
Sex (male)	3.2099	1.2700	8.1126	0.0137*				
Smoking history (>20 pack-years)	2.5801	1.0964	6.0715	0.0299*				
Histology (non-adenocarcinoma)	6.2112	2.3251	16.5924	0.0003**	4.2469	1.4132	12.7629	0.0100**
TNM Stage (UICC-7) (II/III)	4.2078	1.7387	10.1834	0.0014**				
Size (>30 mm)	2.9184	1.2481	6.8238	0.0135*				
Lymph node metastasis (pN1-3)	5.3148	1.8990	14.8744	0.0015**	5.2127	1.6251	16.7206	0.0055**
Lymph invasion	1.4143	0.6010	3.3279	0.4272				
Venous invasion	0.9500	0.3240	2.7859	0.9256				
Pleural invasion	2.2689	0.9952	5.1730	0.0514	2.7348	1.0001	7.4786	0.0500*
EGFR mutation	0.2114	0.0788	0.5669	0.0020**	0.2214	0.0671	0.7309	0.0133*
KRAS mutation	0.9778	0.1871	5.1085	0.9787				

Values with statistical significance were indicated with *($p < 0.05$) or **($p < 0.01$). NU: Nagoya University Hospital; CI: confidence interval.
[a] Logistic regression analysis.

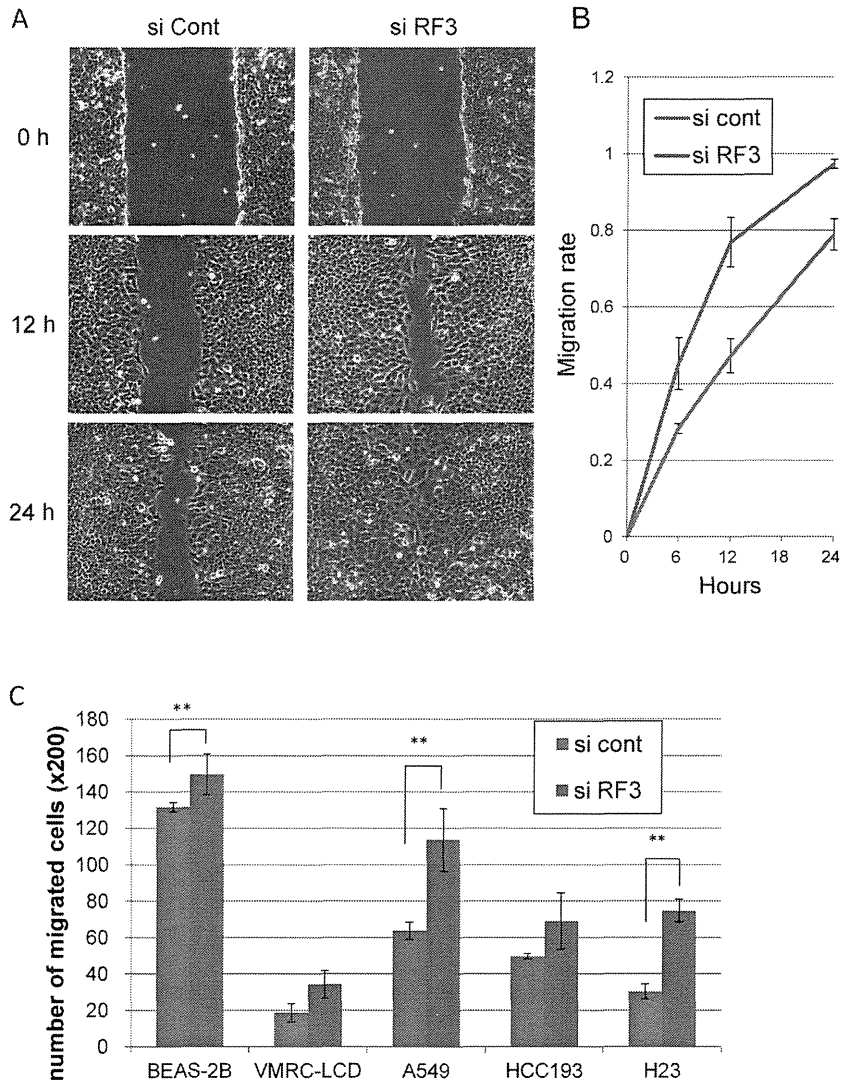

Fig. 2. RASSF3 knockdown enhances cell motility in the wound healing assay (A and B) and transwell migration assay (C). (A) Forty-eight hours after the transfection, A549 cells were re-plated in 3.5 cm dishes. After the cells had grown to confluence, cultures were damaged using 1–200 μl beveled orifice tip and then allowed to migrate. Photographs were taken at the indicated time points. (B) Migration rate is designated as a – b/a (a and b represent the widths of the fissures at time 0 and each time point, respectively). RASSF3-knockdown cells increased migration rate compared to the control. (C) Transwell migration assay. Cell lines transfected with siRNA were re-plated into a transwell chamber 48 h after the transfection and cells were counted after 24 h incubation. RASSF3-knockdown statistically significantly enhanced migration ability of 3 cell lines (A549, BEAS-2B, and NCI-H23). Although HCC193 also showed enhancement by RASSF3-knockdown, it was not statistically significant. The migration ability of VMRC-LCD was exceptionally low, and hardly affected by RASSF3-knockdown. si RF3: siRNA against RASSF3; si Cont: negative control siRNA.

3.4. DNA hypermethylation not a main cause of RASSF3 downregulation

In order to determine whether or not low *RASSF3* expression was induced by DNA hypermethylation, we studied the DNA methylation status at the CpG island of the *RASSF3* gene promoter region using lung cancer cell lines. Fourteen lung cancer cell lines showed various *RASSF3* expression levels compared with an immortalized normal bronchial epithelial cell line BEAS-2B, the majority of which showed lower expression than in BEAS-2B (Supplemental Fig. 3A). However, we detected no CpG island methylation in the promoter region of the *RASSF3* gene in 14 lung cancer cell lines (Supplemental Fig. 3B). We also examined 8 NSCLC clinical samples from the low *RASSF3* expression group. However, we could not find DNA methylation in any specimens. These results suggested that DNA hypermethylation was not a major cause of *RASSF3* downregulation (Supplemental Fig. 3C).

3.5. Silence of RASSF3 increases migration rate in NSCLC cells

The above results suggested that RASSF3 downregulation was associated with more malignant phenotypes including lymph node metastasis. To determine whether RASSF3 suppression promotes lung cancer cell migration ability in vitro, we transfected either RASSF3 targeted or control siRNA into four lung cancer cell lines (A549, HCC193, NCI-H23, and VMRC-LCD) and one immortalized bronchial epithelial cell line (BEAS-2B), and conducted wound healing and transwell migration assays. In the wound healing assay, migration ability was increased in RASSF3-knockdown A549 cells compared to the control cells (Fig. 2A and B). Similar results were obtained with three other cell lines including BEAS-2B, NCI-H23, and HCC193 (Supplemental Fig. S4). Similarly, in the transwell migration assay, RASSF3-knockdown enhanced migration ability of those 4 cell lines (A549, HCC193, NCI-H23, and BEAS-2B), although the enhancement in HCC193 was not statistically significant (Fig. 2C

and Supplemental Fig. S5). Because the migration ability of VMRC-LCD was exceptionally low, the effect of RASSF3-knockdown can be hardly evaluated in this cell line (Fig. 2C, Supplemental Figs. S4D, S4H, and S5).

4. Discussion

In the present study, we demonstrated that *RASSF3* expression was frequently downregulated in NSCLCs. Decrease of its expression was significantly associated with the progressive phenotypes of lung cancer including lymph node metastasis and pleural invasion. The strong correlation of lower *RASSF3* expression with such malignant phenotypes may imply that *RASSF3* downregulation plays an important role in cancer cell migration or invasion. This idea is supported by our in vitro studies which showed that RASSF3 knockdown promoted cell migration abilities of lung cancer cell lines. In this regard, we previously reported that RASSF3 stabilized p53 [16], and p53 was also shown to negatively regulate epithelial to mesenchymal transition (EMT) induced by TGF-β [20]. One possible mechanism of the tumor suppressive activity of RASSF3 might be a negative control of EMT through p53 stabilization. In this regard, EMT induction has been indicated to account for increased cancer cell migration/invasion [21]. However, although our preliminary in vitro experiments were suggestive, they failed to provide sufficient evidence to confirm EMT induction in the lung cancer cells by RASSF3-knockdown (data not shown).

The low *RASSF3* expression group also showed a correlation with wild-type *EGFR* status in univariate analysis. Multivariate analysis also revealed this correlation between RASSF3 and EGFR, indicating that this relationship was independent from other parameters. These data might suggest that the signaling pathways were regulated by RASSF3 and EGFR crosstalk in-between, and thus the alteration or mutation of each gene is mutually exclusive. On this point, Cui et al. reported that desmocollin 3, the target gene of p53, inhibits the EGFR/ERK pathway in human lung cancer [22]. Since RASSF3 stabilizes p53 [16], RASSF3 silencing might downregulate desmocollin 3 expression through p53 destabilization, resulting in activation of the EGFR/ERK pathway. However, further studies are needed to clarify whether or not such an interaction between the EGFR and RASSF3 signaling exists.

We found no significant correlation between *RASSF3* expression and patients' survival. This seemed to contradict the significant correlation of *RASSF3* with lymph node metastasis or pleural invasion in this study, where both were strong predictors of poor prognosis [23–25]. In this regard, previous studies reported that postoperative therapy has a strong influence on patients' survival, which we had earlier suspected to explain this inconsistency [26,27]. However, we found no remarkable difference in postoperative treatment between the two expression groups. Although we conducted further subset analyses of various kinds to explain this discrepancy, no significant factors were identified.

Finally, to determine the underlying mechanisms of *RASSF3* downregulation, we examined 14 lung cancer cell lines and 8 lung tumor specimens from the low expression group. However, we found no methylation of CpGs in the *RASSF3* promoter region. Previous studies also reported no methylation of *RASSF3* in 8 colorectal cancer cell lines, 8 thyroid cancer cell lines or 6 glioma cell lines [28–30]. Thus, simple hypermethylation of the promoter region may not be the primary mechanism to suppress RASSF3 transcription.

In conclusion, the present study showed that RASSF3 is frequently downregulated in NSCLCs, leading to an increase in lymph node metastasis or pleural invasion. These results indicate that RASSF3 is a tumor suppressor of lung cancer. Furthermore, the possible interaction between the RASSF3 and EGFR signaling might give new clues to dissect the complicated pathogenesis of lung cancer, which has long been virtually insurmountable riddle.

Conflict of interest statement

None declared.

Acknowledgments

This work was supported in part by JSPS KAKENHI (22300338, 2465065 YS, 23790725 KN, 22590267 YH), and a Grant-in-Aid for Third-Term Comprehensive Control Research for Cancer from the Ministry of Health, Labor and Welfare of Japan, and the Takeda Science Foundation (YS, KN). We thank Ms. Miwako Nishizawa for her excellent technical assistance.

Appendix A. Supplementary data

Supplementary data associated with this article can be found, in the online version, at http://dx.doi.org/10.1016/j.lungcan.2013.10.014.

References

[1] Jemal A, Bray F, Center MM, Ferlay J, Ward E, Forman D. Global cancer statistics. CA Cancer J Clin 2011;61:69–90.
[2] Richter AM, Pfeifer GP, Dammann RH. The RASSF proteins in cancer; from epigenetic silencing to functional characterization. Biochim Biophys Acta 2009;1796:114–28.
[3] Pfeifer GP, Dammann R, Tommasi S. RASSF proteins. Curr Biol 2010;20:R344–5.
[4] Sherwood V, Recino A, Jeffries A, Ward A, Chalmers AD. The N-terminal RASSF family: a new group of Ras-association-domain-containing proteins, with emerging links to cancer formation. Biochem J 2010;425:303–11.
[5] Underhill-Day N, Hill V, Latif F. N-terminal RASSF family: RASSF7-RASSF10. Epigenetics 2011;6:284–92.
[6] Dammann R, Li C, Yoon JH, Chin PL, Bates S, Pfeifer GP. Epigenetic inactivation of a RAS association domain family protein from the lung tumour suppressor locus 3p21.3. Nat Genet 2000;25:315–9.
[7] Burbee DG, Forgacs E, Zochbauer-Muller S, Shivakumar L, Fong K, Gao B, et al. Epigenetic inactivation of RASSF1A in lung and breast cancers and malignant phenotype suppression. J Natl Cancer Inst 2001;93:691–9.
[8] Endoh H, Yatabe Y, Shimizu S, Tajima K, Kuwano H, Takahashi T, et al. RASSF1A gene inactivation in non-small cell lung cancer and its clinical implication. Int J Cancer 2003;106:45–51.
[9] Ito M, Ito G, Kondo M, Uchiyama M, Fukui T, Mori S, et al. Frequent inactivation of RASSF1A, BLU, and SEMA3B on 3p21.3 by promoter hypermethylation and allele loss in non-small cell lung cancer. Cancer Lett 2005;225:131–9.
[10] Wang J, Wang B, Chen X, Bi J. The prognostic value of RASSF1A promoter hypermethylation in non-small cell lung carcinoma: a systematic review and meta-analysis. Carcinogenesis 2011;32:411–6.
[11] Jo H, Kim JW, Kang GH, Park NH, Song YS, Kang SB, et al. Association of promoter hypermethylation of the RASSF1A gene with prognostic parameters in endometrial cancer. Oncol Res 2006;16:205–9.
[12] Ma L, Zhang JH, Liu FR, Zhang X. Hypermethylation of promoter region of RASSF1A gene in ovarian malignant epithelial tumors. Zhonghua Zhong Liu Za Zhi 2005;27:657–9.
[13] Sugawara W, Haruta M, Sasaki F, Watanabe N, Tsunematsu Y, Kikuta A, et al. Promoter hypermethylation of the RASSF1A gene predicts the poor outcome of patients with hepatoblastoma. Pediatr Blood Cancer 2007;49:240–9.
[14] Tommasi S, Dammann R, Jin SG, Zhang XF, Avruch J, Pfeifer GP. RASSF3 and NORE1: identification and cloning of two human homologues of the putative tumor suppressor gene RASSF1. Oncogene 2002;21:2713–20.
[15] Jacquemart IC, Springs AE, Chen WY. Rassf3 is responsible in part for resistance to mammary tumor development in neu transgenic mice. Int J Oncol 2009;34:517–28.
[16] Kudo T, Ikeda M, Nishikawa M, Yang Z, Ohno K, Nakagawa K, et al. The RASSF3 candidate tumor suppressor induces apoptosis and G1-S cell-cycle arrest via p53. Cancer Res 2012;72:2901–11.
[17] Paez JG, Janne PA, Lee JC, Tracy S, Greulich H, Gabriel S, et al. EGFR mutations in lung cancer: correlation with clinical response to gefitinib therapy. Science 2004;304:1497–500.
[18] Pao W, Miller V, Zakowski M, Doherty J, Politi K, Sarkaria I, et al. EGF receptor gene mutations are common in lung cancers from never smokers and are associated with sensitivity of tumors to gefitinib and erlotinib. Proc Natl Acad Sci U S A 2004;101:13306–11.
[19] Shigematsu H, Lin L, Takahashi T, Nomura M, Suzuki M, Wistuba II, et al. Clinical and biological features associated with epidermal growth factor receptor gene mutations in lung cancers. J Natl Cancer Inst 2005;97:339–46.

[20] Termen S, Tan EJ, Heldin CH, Moustakas A. p53 regulates epithelial-mesenchymal transition induced by transforming growth factor beta. J Cell Physiol 2013;228:801–13.
[21] Thomson S, Petti F, Sujka-Kwok I, Mercado P, Bean J, Monaghan M, et al. A systems view of epithelial-mesenchymal transition signaling states. Clin Exp Metastasis 2011;28:137–55.
[22] Cui T, Chen Y, Yang L, Knosel T, Huber O, Pacyna-Gengelbach M, et al. The p53 target gene desmocollin 3 acts as a novel tumor suppressor through inhibiting EGFR/ERK pathway in human lung cancer. Carcinogenesis 2012;33:2326–33.
[23] Fukui T, Mori S, Yokoi K, Mitsudomi T. Significance of the number of positive lymph nodes in resected non-small cell lung cancer. J Thorac Oncol 2006;1:120–5.
[24] Shimizu K, Yoshida J, Nagai K, Nishimura M, Ishii G, Morishita Y, et al. Visceral pleural invasion is an invasive and aggressive indicator of non-small cell lung cancer. J Thorac Cardiovasc Surg 2005;130:160–5.
[25] Kanzaki R, Ikeda N, Okura E, Kitahara N, Shintani Y, Okimura A, et al. Surgical results and staging of non-small cell lung cancer with interlobar pleural invasion. Interact Cardiovasc Thorac Surg 2012;14:739–42.
[26] Heon S, Johnson BE. Adjuvant chemotherapy for surgically resected non-small cell lung cancer. J Thorac Cardiovasc Surg 2012;144: S39–42.
[27] Tsuboi M, Ohira T, Saji H, Miyajima K, Kajiwara N, Uchida O, et al. The present status of postoperative adjuvant chemotherapy for completely resected non-small cell lung cancer. Ann Thorac Cardiovasc Surg 2007;13: 73–7.
[28] Hesson LB, Wilson R, Morton D, Adams C, Walker M, Maher ER, et al. CpG island promoter hypermethylation of a novel Ras-effector gene RASSF2A is an early event in colon carcinogenesis and correlates inversely with K-ras mutations. Oncogene 2005;24:3987–94.
[29] Schagdarsurengin U, Richter AM, Hornung J, Lange C, Steinmann K, Dammann RH. Frequent epigenetic inactivation of RASSF2 in thyroid cancer and functional consequences. Mol Cancer 2010;9:264.
[30] Hesson L, Bieche I, Krex D, Criniere E, Hoang-Xuan K, Maher ER, et al. Frequent epigenetic inactivation of RASSF1A and BLU genes located within the critical 3p21.3 region in gliomas. Oncogene 2004;23:2408–19.

Published OnlineFirst January 27, 2014; DOI: 10.1158/2159-8290.CD-13-0633

CANCER DISCOVERY

CD74–NRG1 Fusions in Lung Adenocarcinoma

Lynnette Fernandez-Cuesta, Dennis Plenker, Hirotaka Osada, et al.

Cancer Discovery 2014;4:415-422. Published OnlineFirst January 27, 2014.

Published OnlineFirst January 27, 2014; DOI: 10.1158/2159-8290.CD-13-0633

RESEARCH BRIEF

CD74–NRG1 Fusions in Lung Adenocarcinoma

Lynnette Fernandez-Cuesta[1], Dennis Plenker[1], Hirotaka Osada[19], Ruping Sun[13], Roopika Menon[9,14], Frauke Leenders[1,3], Sandra Ortiz-Cuaran[1], Martin Peifer[1,5], Marc Bos[1], Juliane Daßler[15], Florian Malchers[1], Jakob Schöttle[1,10], Wenzel Vogel[14], Ilona Dahmen[1], Mirjam Koker[1], Roland T. Ullrich[2,10], Gavin M. Wright[21], Prudence A. Russell[22], Zoe Wainer[21], Benjamin Solomon[23], Elisabeth Brambilla[24], Hélène Nagy-Mignotte[25], Denis Moro-Sibilot[25], Christian G. Brambilla[25], Sylvie Lantuejoul[24], Janine Altmüller[6,7,12], Christian Becker[6], Peter Nürnberg[5,6,7], Johannes M. Heuckmann[9], Erich Stoelben[11], Iver Petersen[16], Joachim H. Clement[17], Jörg Sänger[18], Lucia A. Muscarella[26], Annamaria la Torre[26], Vito M. Fazio[26,27], Idoya Lahortiga[28], Timothy Perera[29], Souichi Ogata[29], Marc Parade[29], Dirk Brehmer[29], Martin Vingron[13], Lukas C. Heukamp[8], Reinhard Buettner[3,4,8], Thomas Zander[1,2,4], Jürgen Wolf[2,3,4], Sven Perner[14], Sascha Ansén[2], Stefan A. Haas[13], Yasushi Yatabe[20], and Roman K. Thomas[1,3,8]

ABSTRACT We discovered a novel somatic gene fusion, *CD74–NRG1*, by transcriptome sequencing of 25 lung adenocarcinomas of never smokers. By screening 102 lung adenocarcinomas negative for known oncogenic alterations, we found four additional fusion-positive tumors, all of which were of the invasive mucinous subtype. Mechanistically, CD74–NRG1 leads to extracellular expression of the EGF-like domain of NRG1 III-β3, thereby providing the ligand for ERBB2–ERBB3 receptor complexes. Accordingly, ERBB2 and ERBB3 expression was high in the index case, and expression of phospho-ERBB3 was specifically found in tumors bearing the fusion ($P < 0.0001$). Ectopic expression of CD74–NRG1 in lung cancer cell lines expressing ERBB2 and ERBB3 activated ERBB3 and the PI3K–AKT pathway, and led to increased colony formation in soft agar. Thus, *CD74–NRG1* gene fusions are activating genomic alterations in invasive mucinous adenocarcinomas and may offer a therapeutic opportunity for a lung tumor subtype with, so far, no effective treatment.

SIGNIFICANCE: *CD74–NRG1* fusions may represent a therapeutic opportunity for invasive mucinous lung adenocarcinomas, a tumor with no effective treatment that frequently presents with multifocal unresectable disease. *Cancer Discov; 4(4); 415–22. ©2014 AACR.*

Authors' Affiliations: [1]Department of Translational Genomics; [2]Department I of Internal Medicine; [3]Laboratory of Translational Cancer Genomics; [4]Network Genomic Medicine, University Hospital Cologne, Center of Integrated Oncology Cologne-Bonn; [5]Center for Molecular Medicine Cologne (CMMC); [6]Cologne Center for Genomics (CCG); [7]Cologne Excellence Cluster on Cellular Stress Responses in Aging-Associated Diseases (CECAD); [8]Department of Pathology, University Hospital Medical Center, University of Cologne; [9]Blackfield AG; [10]Max Planck Institute for Neurological Research; [11]Thoracic Surgery, Lungenklinik Merheim, Kliniken der Stadt Köln gGmbH; [12]Institute of Human Genetics, Cologne; [13]Computational Molecular Biology Department, Max Planck Institute for Molecular Genetics, Berlin; [14]Department of Prostate Cancer Research, Institute of Pathology; [15]Institute for Clinical Chemistry and Clinical Pharmacology, University Hospital Bonn, Bonn; [16]Institute of Pathology; [17]Department of Internal Medicine II, Jena University Hospital, Friedrich-Schiller-University, Jena; [18]Institute for Pathology Bad Berka, Bad Berka, Germany; [19]Division of Molecular Oncology, Aichi Cancer Center Research Institute; [20]Department of Pathology and Molecular Diagnostics, Aichi Cancer Center, Nagoya, Japan; Departments of [21]Surgery and [22]Pathology, St. Vincent's Hospital; [23]Department of Haematology and Medical Oncology, Peter MacCallum Cancer Centre, Melbourne, Victoria, Australia; [24]Department of Pathology, [25]CHU Grenoble Institut National de la Santé et de la Recherche Medicale (INSERM) U823, Institute Albert Bonniot, Grenoble-Alpes University, Grenoble, France; [26]Laboratory of Oncology IRCCS Casa Sollievo della Sofferenza, San Giovanni Rotondo; [27]Laboratory for Molecular Medicine and Biotechnology, University Campus Bio-Medico, Rome, Italy; [28]Center for the Biology of Disease, VIB, Leuven; and [29]Oncology Discovery, Janssen Research and Development, A Division of Janssen Pharmaceutica NV, Beerse, Belgium

Note: Supplementary data for this article are available at Cancer Discovery Online (http://cancerdiscovery.aacrjournals.org/).

L. Fernandez-Cuesta and D. Plenker contributed equally to this work.

Corresponding Author: Roman K. Thomas, Department of Translational Genomics, Medical Faculty, University of Cologne, Weyertal 115b, 50931 Cologne, Germany. Phone: 49-221-478-98771; Fax: 49-221-478-97902; E-mail: roman.thomas@uni-Koeln.de

doi: 10.1158/2159-8290.CD-13-0633

Published OnlineFirst January 27, 2014; DOI: 10.1158/2159-8290.CD-13-0633

INTRODUCTION

Lung adenocarcinomas of patients who have never smoked frequently bear kinase gene alterations, such as *EGFR* mutations and translocations affecting *ALK*, *ROS1*, and *RET* (1–6). These alterations cause "oncogene dependency" on the activated kinase and, thus, sensitivity of the tumor cells to kinase inhibitors. Patients whose tumors bear kinase gene alterations can be effectively treated with an ever-growing number of kinase inhibitors; for example, patients with *EGFR*-mutant lung cancer treated with EGF receptor (EGFR) inhibitors have a significantly longer progression-free survival compared with patients treated with conventional chemotherapy (7). Similarly, ALK and ROS1 inhibition induces clinically relevant remissions in patients bearing the respective genomic fusion (8–10). Unfortunately, despite substantive cancer genome sequencing efforts, a majority of lung tumors still lack therapeutically tractable kinase alterations (1). We therefore sought to identify novel therapeutically relevant driver alterations in otherwise driver-negative lung adenocarcinomas.

RESULTS

We collected a cohort of 25 lung adenocarcinoma specimens of never smokers that lacked mutations in *KRAS* or *EGFR*, on which we performed chromosomal gene copy-number analysis as well as transcriptome sequencing with the aim of identifying new oncogenic driver alterations. We applied a novel computational data analysis strategy that combines split-read and read-pair analyses with *de novo* assembly of candidate regions containing potential breakpoints to achieve sensitive and accurate detection of fusion transcripts (see Methods; Fernandez-Cuesta and colleagues, published elsewhere). Of the 25 samples analyzed (Supplementary Table S1), 10 carried a known oncogene. One sample exhibited *EGFR* amplification, paralleled by overexpression of the gene (Fig. 1A and Supplementary Fig. S1). We also found 3 cases each of *ALK*, *ROS1*, and *RET* fusions (Fig. 1A and Supplementary Table S2). In addition, we detected one sample carrying a novel chimeric transcript fusing the first six exons of *CD74* to the exons encoding the EGF-like domain of the neuregulin-1 (NRG1) III-β3 isoform (Fig. 1A and B and Supplementary Table S2). This fusion raised our interest because *CD74* is part of recurrent fusions affecting the *ROS1* (3) kinase in lung adenocarcinoma, and because *NRG1* encodes a ligand of ERBB receptor tyrosine kinases, which are also frequently affected by genome alterations in this tumor type. NRG1 provides the ligand for ERBB3 and ERBB4 receptors (11). The NRG1 isoform present in our fusion transcript belongs to the type III and carries the EGF-like domain type β, which has higher affinity to the receptors than the α-type (12). NRG1 type III expression is mostly limited to neurons and is the only isoform displaying this degree of tissue-specific expression (13). Only the sample carrying the *CD74–NRG1* fusion exhibited high expression of the NRG1 III-β3 isoform [74 fragments per kilobase per million reads (FPKM); Fig. 1C, top; Supplementary Table S3], and in this specimen there was no expression of the wild-type allele (Fig. 1C, bottom). In addition, NRG1 was generally not expressed in lung adenocarcinoma as shown by transcriptome sequencing data of our cohort of 25 lung adenocarcinomas of never smokers (Fig. 1C, top, and Supplementary Table S3), and of a cohort of 15 unselected lung adenocarcinomas (Fig. 1C, top, and Supplementary Table S4). The fusion resulted from a somatic genomic event as *CD74–NRG1* fusion FISH and *NRG1* break-apart FISH revealed rearrangements in the respective chromosomal regions in the tumor cells, but not in surrounding nontumoral cells (Fig. 1D and Supplementary Fig. S2). Furthermore, by applying hybrid-capture–based massively parallel genomic sequencing (Fig. 1D and Supplementary Table S5), we found five and two reads spanning and encompassing the chromosomal breakpoint (chr5:149,783,493 and chr8:32,548,502), respectively.

We next performed reverse transcriptase PCR (RT-PCR) using primers specific for the chimeric transcript to identify additional tumors bearing the fusion in a set of 102 pan-negative adenocarcinomas of never smokers (wild-type for *EGFR*, *KRAS*, *BRAF*, *ERBB2*, *ALK*, *ROS*, and *RET* genes). We identified four additional tumors carrying the fusion (Supplementary Table S6), which were also confirmed by break-apart FISH. All 5 cases (including the index case) occurred in invasive mucinous adenocarcinomas (IMA) of women who had never smoked (Fig. 2A). Invasive mucinous lung adenocarcinoma is highly associated with *KRAS* mutations (14). Indeed, out of 15 invasive mucinous lung adenocarcinoma specimens (all derived from an East Asian population), six carried a *KRAS* mutation (40%), and four carried the *CD74–NRG1* fusion (27%; Fig. 2B; Supplementary Table S7). We additionally tested other lung tumor subtypes (63 cases), as well as four other cancer types (21 cases) and all were negative for the fusion gene (Supplementary Table S6), suggesting a strong link between the presence of *CD74–NRG1* and invasive mucinous adenocarcinoma.

Characteristic features of type III NRG1 are cytosolic N-termini and membrane-tethered EGF-like domains (13, 15). In the case of CD74–NRG1, the part of CD74 is predicted to replace the transmembrane domain present in wild-type NRG1 III-β3, preserving the membrane-tethered EGF-like domain (Fig. 2C). To validate this prediction, we transduced NIH-3T3 cells with CD74–NRG1-encoding retroviruses, and performed flow cytometry analyses to determine the subcellular distribution of expression of the fusion protein. As expected, we observed a positive intracellular (but not extracellular) signal for CD74 (Fig. 2D, left) and a positive extracellular signal for NRG1 (Fig. 2D, right). Similar results were observed in H2052 cells (Supplementary Fig. S3). Furthermore, we were unable to detect the fusion in the supernatant of transduced cells with a polyclonal antibody raised against the EGF-like domain (data not shown). Thus, the fusion does not lead to secretion of the EGF-like domain, but probably generates a membrane-bound protein with the EGF-like domain presented on the outside of the cell.

We next analyzed the expression of ERBB receptors in the index case: *ERBB1* (*EGFR*) was almost not expressed (FPKM = 1.9; Fig. 3A; Supplementary Table S8; Supplementary Fig. S4) and not phosphorylated (Supplementary Fig. S4). In contrast, *ERBB2* was expressed (FPKM = 22.9; Fig. 3A; Supplementary Table S8) and phosphorylated (Fig. 3B, left); similar to *ERBB2*, *ERBB3* was also expressed at relatively high levels

Published OnlineFirst January 27, 2014; DOI: 10.1158/2159-8290.CD-13-0633

A

Sample	Age	Sex	Stage	Driver
Case-01	63	Female	Ia	*EGFR*-amp
Case-08	68	Male	Ia	*EML4–ALK*
Case-10	46	Female	Ia	*EML4–ALK*
Case-17	39	Female	IIIa	*EML4–ALK*
Case-06	56	Female	IIIb	*CD74–ROS1*
Case-09	60	Female	Ia	*CD74–ROS1*
Case-02	68	Female	IIIb	*EZR–ROS1*
Case-15	65	Female	IIa	*KIF5B–RET*
Case-25	75	Male	Ia	*KIF5B–RET*
Case-23	66	Female	IIIb	*CCDC6–RET*
Case-19*	64	Female	Ib	*CD74–NRG1*
Case-03	72	Female	IV	
Case-04	74	Male	IV	
Case-05	50	Female	IV	
Case-07	70	Female	Ia	
Case-11	79	Female	IIa	
Case-12	72	Male	IV	
Case-13	59	Male	Ib	Unknown
Case-14	63	Female	IIIa	
Case-16	48	Male	IIIb	
Case-18	71	Female	IIIa	
Case-20	74	Female	IIIa	
Case-21	73	Male	Ib	
Case-22	80	Female	Ib	
Case-24	66	Female	IIIa	

*, Index case (Caucasian, invasive mucinous adenocarcinoma)

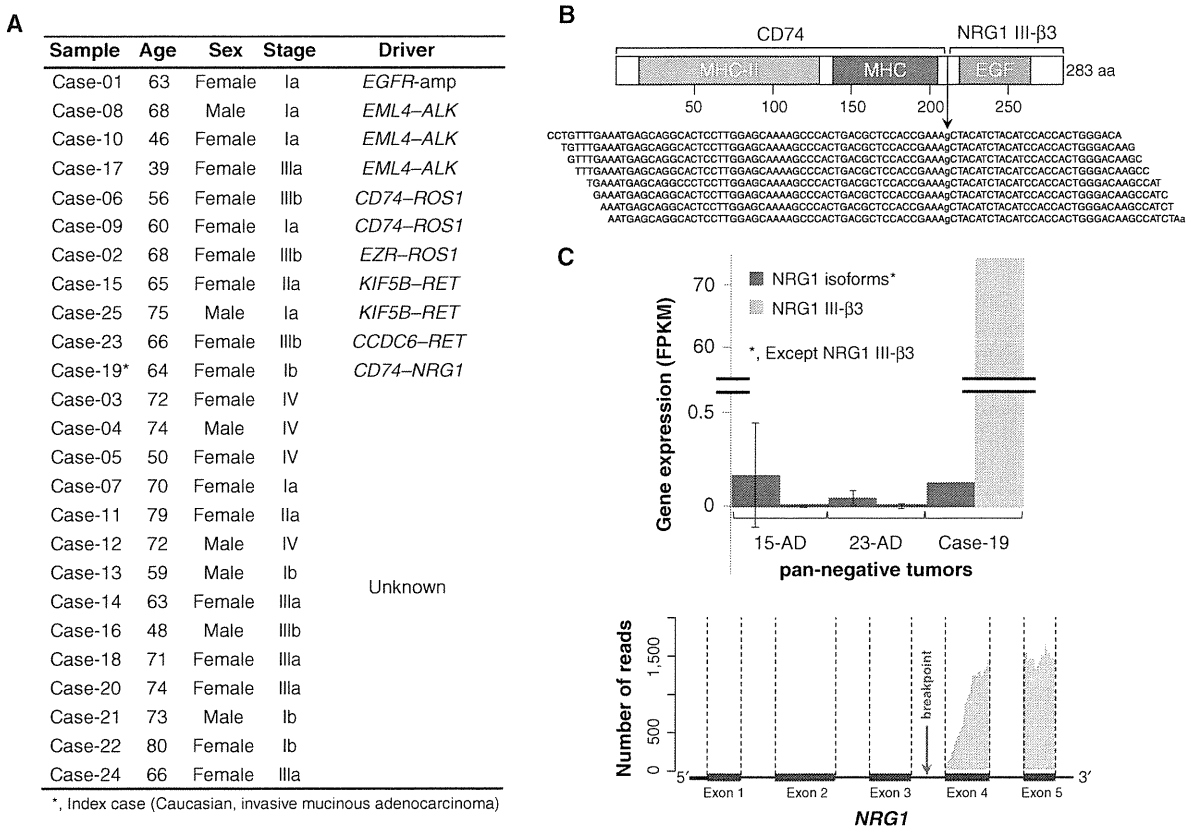

Figure 1. Identification of the *CD74-NRG1* fusion gene. **A,** overview of driver genes detected in a cohort of 25 *EGFR*- and *KRAS*-negative lung adenocarcinomas of never smokers. **B,** detection of *CD74-NRG1* fusion transcript by transcriptome sequencing. Schematic representation of the fusion transcript domains and some of the transcriptome sequencing reads spanning the fusion point. **C,** expression levels of *NRG1* isoforms in 15 unselected and 23 pan-negative lung adenocarcinomas (AD; wild-type for *EGFR*, *KRAS*, *BRAF*, *ERBB2*, *ALK*, *ROS*, and *RET*), and, in the index case, inferred from transcriptome sequencing data. Average FPKM values are shown (top). RNAseq analysis for *NRG1* reads to show where the breakpoint of *CD74-NRG1* occurs. The dip in exon 4 represents reads of the fusion that could not be mapped. No reads could be mapped to exons 1–3 (bottom). **D,** top, the genomic intron/exon structure of the *CD74* (in green) and the *NRG1* locus (in orange) with the genomic breakpoints marked in red. Sequencing reads were obtained from hybrid-capture–based genomic sequencing of 333 genes using genomic DNA of the index case (see Methods). The breakpoint-spanning reads are shown by means of the Integrative Genomics Viewer (www.broadinstitute.org/igv/) focused on the *CD74* gene (bottom). The gray area of the read is aligned to the *CD74* reference sequence. Colored area on the right indicates bases not matching the *CD74* reference sequence. Sequence comparison reveals alignment to the *NRG1* reference sequence. Encompassing reads whose mate pairs are mapped to the *NRG1* locus on chromosome 8 are displayed in dark purple. Bottom, a representative picture of *NRG1* break-apart FISH. Arrows, break-apart signals.

Published OnlineFirst January 27, 2014; DOI: 10.1158/2159-8290.CD-13-0633

A

Sample	Age	Sex	Stage	Smoking status	AD subtype
Index-case	64	Female	Ib	Never	Invasive mucinous
Case-A	73	Female	Ia	Never	Invasive mucinous
Case-B	72	Female	Ia	Never	Invasive mucinous
Case-C	66	Female	Ia	Never	Invasive mucinous
Case-D	31	Female	Ia	Never	Invasive mucinous

EGFR, KRAS, BRAF, HER2, ALK, ROS, RET negative

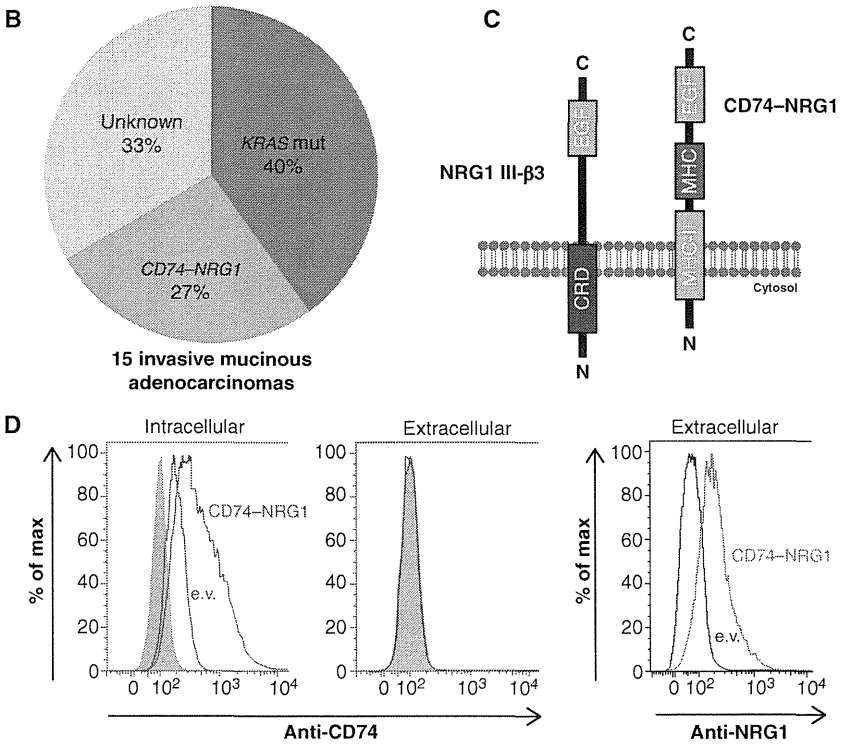

Figure 2. Association of *CD74-NRG1* with invasive mucinous adenocarcinoma, and membrane localization of the fusion protein. **A,** clinical characteristics of the index case and the 4 additional cases found to harbor *CD74-NRG1*. **B,** frequency of *KRAS* mutations and *CD74-NRG1* rearrangements in a cohort of 15 IMA tumors (East Asian population). **C,** schematic representation of wild-type NRG1 III-β3 and predicted CD74-NRG1 fusion protein in the cellular membrane. **D,** intracellular and extracellular staining of CD74 (left), and extracellular staining of NRG1 (right) in CD74-NRG1-transduced NIH-3T3 cells, detected by flow cytometry. The percentage of max is the number of cells in each bin divided by the number of cells in the bin that contains the largest number of cells. e.v., empty vector control.

(FPKM = 22.8; Fig. 3A; Supplementary Table S8) and also phosphorylated (Fig. 3B, right). *ERBB4* was not expressed in the index case (FPKM = 0.2; Fig. 3A; Supplementary Table S8). To our surprise, expression of phosphorylated ERBB3 (p-ERBB3) was almost exclusively restricted to fusion-positive cases, as determined by an immunohistochemical analysis of a tissue microarray containing 241 unselected adenocarcinomas. Although a positive signal was detected for p-ERBB3 in the five CD74-NRG1-positive invasive mucinous adenocarcinomas, only six of 241 unselected adenocarcinomas exhibited detectable levels of p-ERBB3 ($P < 0.0001$; Fig. 3C). Together, these observations support the notion that CD74-NRG1 might provide the ligand for ERBB2-ERBB3 heterodimers, thus activating the phosphoinositide 3-kinase (PI3K)-AKT pathway, as previously shown for wild-type NRG1 (16).

To formally test this hypothesis, we transduced different cell lines with retroviruses encoding CD74-NRG1 and performed Western blot analyses under starving conditions. Because NIH-3T3 cells have low-to-absent expression of ERBB receptors, and NIH-3T3 cells ectopically expressing ERBB2 and ERBB3 are already oncogenic (Supplementary Fig. S5), we decided to use H322 and H1568 lung cancer cell lines expressing normal ERBB2 and ERBB3 levels instead. We transduced these cell lines with either an empty vector, a virus containing the full fusion transcript, or a virus containing a truncated version of the fusion lacking the EGF-like domain (Supplementary Fig. S6). We observed that H322 and H1568 cell lines ectopically expressing CD74-NRG1 showed increased levels of p-ERBB2, p-ERBB3, p-AKT, and p-S6K when compared with the empty vector control (Fig. 3D). Furthermore, both p-ERBB3 and

Published OnlineFirst January 27, 2014; DOI: 10.1158/2159-8290.CD-13-0633

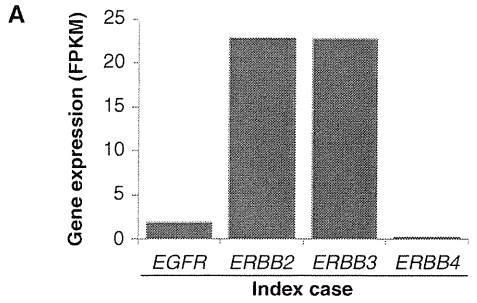

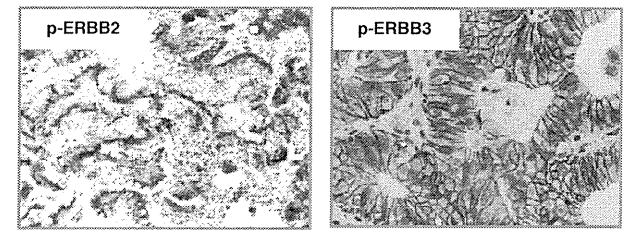

C

p-ERBB3	*CD74–NRG1* (*n* = 5)	AD cohort (*n* = 241)
Positive	5	6
Negative	0	235
		***P* < 0.0001**

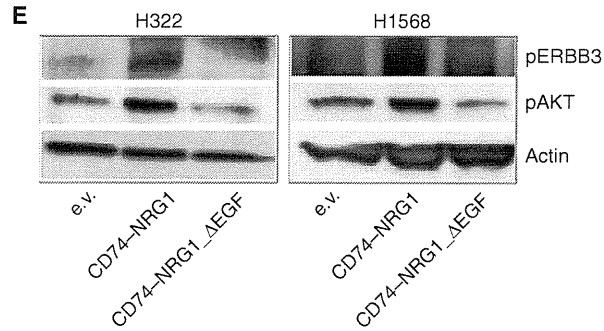

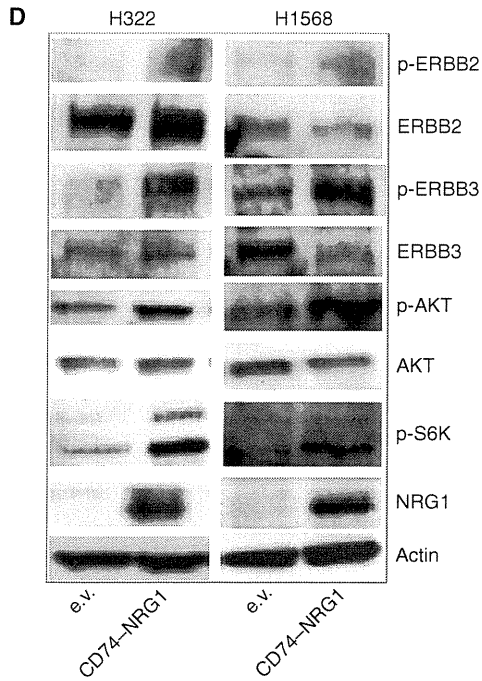

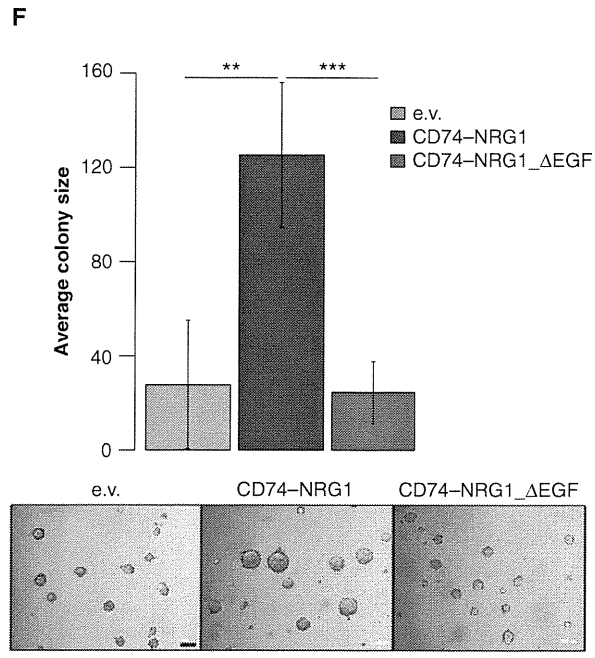

Figure 3. Functional relevance of CD74-NRG1. **A,** expression levels of ERBB receptors in the index case inferred from transcriptome sequencing data. FPKM values are shown. **B,** levels of p-ERBB2 and p-ERBB3 detected by immunohistochemical analysis in a CD74-NRG1-positive case using and antibody directed against ERBB2 Tyr1221/1222 and ERBB2 Tyr1289. **C,** the same p-ERBB3 antibody was used to stain a tissue microarray composed of 241 lung adenocarcinomas. The frequency of p-ERBB3–positive cases in this cohort versus the five CD74-NRG1–positive samples is shown ($P < 0.0001$). **D,** activation of the PI3K-AKT pathway detected by Western blot analysis of H322 and H1568 lung cancer cells transduced with retroviruses encoding CD74-NRG1 or the empty vector control (e.v.). **E,** levels of p-ERBB3 and p-AKT measured by Western blot analysis in the presence of an empty vector, CD74-NRG1, or a truncated version lacking the EGF-like domain (CD74-NRG1_ΔEGF). **F,** anchorage-independent growth of H1568 cells expressing an empty vector, CD74-NRG1, or a truncated version lacking the EGF-like domain (CD74-NRG1_ΔEGF). Top, the average colony size for the three conditions, with error bars representing standard deviations. The experiment was performed with two independent transductions for a total of four times. **, $P < 0.01$; ***, $P < 0.001$. Bottom, representative pictures of the colony formation assay. Please note that H1568 cells are oncogenic and form small colonies without any manipulation.

Published OnlineFirst January 27, 2014; DOI: 10.1158/2159-8290.CD-13-0633

p-AKT depended on the presence of the EGF-like domain of CD74–NRG1 in the fusion (Fig. 3E). In addition, coculture of NIH-3T3 cells ectopically expressing CD74–NRG1 with Ba/F3 cells genetically engineered to express normal ERBB2 and ERBB3 levels also led to activation of AKT (Supplementary Fig. S7). Finally, H1568 cells ectopically expressing CD74–NRG1 exhibited enhanced colony formation in soft-agar assays (Fig. 3F; Supplementary Table S9). Taken together, these data suggest that CD74–NRG1 leads to overexpression of the EGF-like domain of NRG1 III-β3 that acts as a ligand for ERBB3, inducing its phosphorylation and subsequent activation of the downstream PI3K–AKT pathway.

DISCUSSION

We have discovered *CD74–NRG1*, a novel recurrent fusion gene in lung adenocarcinoma that arises from a somatic genomic event. Taking into account the frequencies of mutations of *EGFR* (11.3%), *KRAS* (32.2%), *BRAF* (7%), *ERBB2* (1.7%), or fusions affecting *ALK* (1.3%), *ROS* (1.7%), and *RET* (0.9%; refs. 17, 18) in lung adenocarcinomas, for which our cohort was negative, and the fact that we found 4 positive cases in our validation cohort of 102 pan-negative lung adenocarcinomas, we estimate that the frequency of *CD74–NRG1* in lung adenocarcinomas is approximately 1.7%; however, it is of note that our validation cohort was from an Asian population, so this frequency might be different in Caucasians. *CD74–NRG1* occurred specifically in invasive mucinous lung adenocarcinomas of never smokers, a tumor type that is otherwise associated with *KRAS* mutations (14). In our cohort of limited size (n = 15), *CD74–NRG1* fusions accounted for 27% of invasive mucinous lung adenocarcinomas; together, *KRAS* mutations and *CD74–NRG1* may therefore be considered the causative oncogenes in more than 60% of the cases. We provide evidence that CD74–NRG1 signals through induction of ERBB2–ERBB3 heterodimers, thus leading to PI3K–AKT pathway activation and stimulation of oncogenic growth. In light of the multitude of available drugs targeting ERBB2, ERBB3, and their downstream pathways (19), *CD74–NRG1* fusions may represent a therapeutic opportunity for invasive mucinous lung adenocarcinomas, which frequently present with multifocal and unresectable disease, and for which no effective treatment exists.

METHODS

Sample Preparation, DNA and RNA Extraction, and Illumina Sequencing

Sample preparation and DNA and RNA extraction were performed as previously described (20). RNAseq was performed on cDNA libraries prepared from PolyA+ RNA extracted from tumor cells using the Illumina TruSeq protocol for mRNA. The final libraries were sequenced with a paired-end 2 × 100 bp protocol aiming at 8.5 Gb per sample, resulting in a 30× mean coverage of the annotated transcriptome. All the sequencing was carried on an Illumina HiSeq 2000 sequencing instrument (Illumina).

Analysis of Chromosomal Gene Copy Number (SNP 6.0) and RNAseq Data

Hybridization of the Affymetrix SNP 6.0 arrays was carried out according to the manufacturers' instructions and analyzed using a previously described method (20). For the analysis of RNAseq data, we have developed a pipeline that affords accurate and efficient mapping and downstream analysis of transcribed genes in cancer samples (Fernandez-Cuesta and colleagues; published elsewhere). A brief description of the method was previously provided (20).

Analysis of Targeted Enrichment Genome Sequencing

Genomic DNA was isolated from fresh-frozen tumor tissue and subjected to CAGE Scanner analysis. This approach involves liquid-phase hybrid capture of genomic partitions enriched for genome alterations affecting 333 known cancer-associated genes (also including *CD74*). Subsequent to generation of genomic libraries from tumor DNA and capture, sequencing was performed on the Illumina platform according to the manufacturer's instructions. Significant genomic alterations were identified using approaches described previously (20).

Dideoxy Sequencing

In case of validation, sequencing primer pairs were designed to enclose the putative mutation, or to encompass the candidate rearrangement or chimeric transcript as previously described (20). Sequencing was carried out, and electropherograms were analyzed by visual inspection using four peaks.

Interphase FISH on Formalin-fixed, Paraffin-embedded Sections

Two sets of probes were prepared. One was for break-apart FISH of which probes were mapped at centromeric and telomeric regions between the break point. The other was for fusion FISH that spanned the *NRG1* and *CD74* loci. To intensify the signals, each probe was made of two or three BAC clones as follows, and the probes were labeled with SpectrumGreen and SpectrumOrange (Abbott Molecular-Vysis). Centromeric probes for break-apart FISH were RP11-1002K11 and PR11-25D16. Telomeric probes for break-apart FISH were RP11-23A12 and PR11-715M18. *NRG1* probes for fusion FISH were RP11-715H18, RP11-5713, and PR11-1002K11. *CD74* probes for fusion FISH were PR11-759G10 and PR11-468K14.

Immunohistochemistry

Immunohistochemistry was performed as previously described (21). In brief, the tissue samples were stained with p-ERBB2 (Tyr1221/1222; Cell Signaling Technology) and total ERBB1 (EGFR; Dako) at a dilution of 1:1,000 and 1:50, respectively. The Zeiss MIRAK DESK scanner was used to digitize the stained tissue. Staining for p-EGFR (Tyr1068; Cell Signaling Technology) and p-ERBB3 (Tyr1289; Cell Signaling Technology) was processed with an automated stainer (Autostainer; Dako), using the FLEX+ detection system (Dako).

Cell Culture

H2052, H322, and H1568 cells were obtained from the American Type Culture Collection and maintained in RPMI-1640 medium (Life Technologies) supplemented with 10% fetal calf serum (FCS; Gibco) and 1% penicillin-streptomycin (Gibco). The cells were cultured in a humidified incubator with 5% CO_2 at 37°C. For Western blot analysis experiments, cells were serum starved for 24 hours. NIH-3T3 cells were maintained similarly but in Dulbecco's Modified Eagle Medium (DMEM; Life Technologies). The cells were confirmed to be wild-type for *KRAS*, *EGFR*, *ERBB2*, and *ERBB3* by PCR amplification followed by Sanger sequencing of the PCR products. The cell lines have been authenticated via genotyping (SNP 6.0; Affymetrix) and tested for *Mycoplasma* contamination on a regular basis (MycolAlert; Lonza).

FACS Analysis

NIH-3T3 mouse fibroblast cells were transduced with retrovirus containing empty vector, *CD74–NRG1*, *ERBB2*, *ERBB3*, and *ERBB2+ERBB3*. H2052 cells were transduced with retrovirus

Published OnlineFirst January 27, 2014; DOI: 10.1158/2159-8290.CD-13-0633

containing empty vector or *CD74–NRG1*. Transduced cells (200,000) were washed in fluorescence-activated cell sorting (FACS) buffer (PBS, 2% FCS) and fixed in 4% paraformaldehyde for 30 minutes at room temperature. For permeabilization, cells were washed twice in Saponin buffer (PBS, 0.5% Saponin, and 2% FCS) and intracellular staining of CD74–NRG1 was performed with anti-human-CD74-PE (1:100; BioLegend). Intracellular staining of ERBB2 and ERBB3 was performed with anti-ERBB2 and anti-ERBB3 antibodies (1:50; Cell Signaling Technology). Binding of ERBB2 or ERBB3 was detected with goat-anti-rabbit-Alexa Fluor 488 (Life Technologies). Extracellular staining was performed before permeabilization with anti-human-CD74-PE and anti-NRG1 antibody (1:20; R&D Systems). Binding of the NRG1 part was detected with donkey-anti-goat-Alexa Fluor 488 (Life Technologies). Subsequently, cells were analyzed on a BD LSR II (Beckman Coulter) and quantification was assessed with FlowJo (TreeStar).

Western Blot Analysis

Immunoblotting was performed using standard procedures. The following antibodies were obtained from Cell Signaling Technology: p-AKT Ser473 (Catalog No. #9271), p-P70/S6 (Catalog No. #9205), total ERBB2 (Catalog No. #2242), p-ERBB2 (Catalog No. #2243), total ERBB3 (Catalog No. #4754), and p-ERBB3 (Catalog no. #4791). Anti-human CD74 was obtained from Abcam (Catalog No. # ab22603), and anti-polyclonal NRG1 β 1 was obtained from R&D Systems (Catalog No. AF396-NA). Actin-horseradish peroxidase (HRP) antibody was obtained from Santa Cruz Biotechnology (Catalog No. #sc47778). The antibodies were diluted in 5% BSA/TBST and incubated at 4°C overnight. Proteins were detected with HRP-conjugated anti-mouse, anti-goat, or anti-rabbit antibodies (Millipore) using enhanced chemiluminescence (ECL) reagent (GE Healthcare).

Colony Formation Assay

On a layer of bottom agar (1%), NIH-3T3 cells were suspended at low density in top agar (0.5%) containing 10% FCS, and were grown for 14 days. Subsequently, pictures were taken and systematic analyses were performed with the Scanalyzer (LemnaTec). H1568 cells were cultured under standard conditions in RPMI in 10% FCS and 1% penicillin-streptomycin. p-BABE retroviral vector inserts were confirmed via Sanger sequencing. The cells were generated by at least two independent transductions with retrovirus containing empty vector, *CD74–NRG1*, or *CD74–NRG1_* ΔEGF. After selection for 7 days with puromycin (3 μg/mL), cell lysates were taken for Western blot analysis, and cells were also used for colony formation assays as follows: on a layer of bottom agar (1.2%) cells were suspended at low density in top agar (0.6%) containing 10% FCS (final concentration), and were grown for 14 days. Subsequently, pictures were taken with a Zeiss Axiovert 40 CFL microscope at ×100 magnification, and colony size was assessed with ImageJ (http://rsbweb.nih.gov/ij/).

Generation of Ba/F3_ERBB2+ERBB3 Cells

The *ERBB2* and *ERBB3* open reading frames were amplified by PCR and cloned into the MSCV-puromycin or MSCV-neomycin vectors, respectively (Clonetech). Ba/F3 cells expressing ERBB2 and ERBB3 were generated by retroviral transduction and subsequent puromycin or/and neomycin selection. We verified the expression of the correct proteins by Western blot analysis. Ba/F3 cells were cultured in RPMI-1640 medium supplemented with 10% FBS and 1 ng/mL mouse interleukin-3.

Statistical Analyses

In Fig. 3C and F, we used a two-tailed Fisher exact test.

Disclosure of Potential Conflicts of Interest

L. Fernandez-Cuesta has ownership interest in a patent with the University of Cologne. F. Leenders is a consultant/advisory board member of Blackfield AG. M. Peifer has ownership interest (including patents) in Blackfield AG and is a consultant/advisory board member of the same. F. Malchers is a consultant/advisory board member of One. G.M. Wright has received commercial research support from Covidien and is a consultant/advisory board member of Pfizer. P. Nürnberg is CEO of ATLAS Biolabs GmbH and has ownership interest (including patents) in the same. J.M. Heuckmann is a full-time employee of Blackfield AG and is a co-founder and shareholder of the same. T. Zander is a consultant/advisory board member of Roche, Boehringer Ingelheim, Amgen, and Novartis. R.K. Thomas has received commercial research grants from AstraZeneca, EOS, and Merck KgaA; has ownership interest (including patents) in Blackfield AG and a patent application related to findings in this article; and is a consultant/advisory board member of Blackfield AG, Merck KgaA, Johnson & Johnson, Daiichi-Sankyo, Eli Lilly and Company, Roche, AstraZeneca, Puma, Sanofi, Bayer, Boehringer Ingelheim, and MSD. No potential conflicts of interest were disclosed by the other authors.

Authors' Contributions

Conception and design: L. Fernandez-Cuesta, R.K. Thomas
Development of methodology: L. Fernandez-Cuesta, R. Sun, M. Peifer, J. Altmüller, I. Lahortiga, S. Ogata, M. Parade, D. Brehmer, J. Daßler, S. Ansén, R.K. Thomas
Acquisition of data (provided animals, acquired and managed patients, provided facilities, etc.): L. Fernandez-Cuesta, D. Plenker, H. Osada, R. Menon, F. Leenders, S. Ortiz-Cuaran, M. Bos, J. Daßler, F. Malchers, J. Schöttle, R.T. Ullrich, G.M. Wright, P.A. Russell, Z. Wainer, B. Solomon, H. Nagy-Mignotte, D. Moro-Sibilot, C.G. Brambilla, S. Lantuejoul, J. Altmüller, C. Becker, P. Nürnberg, J.M. Heuckmann, E. Stoelben, J.H. Clement, J. Sänger, L.A. Muscarella, V.M. Fazio, I. Lahortiga, T. Perera, M. Parade, L.C. Heukamp, R. Buettner, T. Zander, J. Wolf, S. Perner, S. Ansén, Y. Yatabe
Analysis and interpretation of data (e.g., statistical analysis, biostatistics, computational analysis): L. Fernandez-Cuesta, D. Plenker, R. Sun, R. Menon, S. Ortiz-Cuaran, F. Malchers, J. Schöttle, R.T. Ullrich, H. Nagy-Mignotte, C.G. Brambilla, J.M. Heuckmann, I. Lahortiga, T. Perera, M. Vingron, J. Wolf, S. Ansén, S.A. Haas, Y. Yatabe, R.K. Thomas
Writing, review, and/or revision of the manuscript: L. Fernandez-Cuesta, D. Plenker, H. Osada, M. Bos, R.T. Ullrich, G.M. Wright, P.A. Russell, Z. Wainer, B. Solomon, E. Brambilla, D. Moro-Sibilot, J. Altmüller, C. Becker, P. Nürnberg, E. Stoelben, D. Brehmer, M. Vingron, R. Buettner, J. Wolf, S. Perner, S. Ansén, Y. Yatabe, R.K. Thomas
Administrative, technical, or material support (i.e., reporting or organizing data, constructing databases): L. Fernandez-Cuesta, D. Plenker, F. Leenders, S. Ortiz-Cuaran, M. Peifer, J. Daßler, F. Malchers, W. Vogel, M. Koker, G.M. Wright, P. Nürnberg, J.M. Heuckmann, I. Petersen, J.H. Clement, J. Sänger, S. Ogata, L.C. Heukamp, R. Buettner, S. Perner, S. Ansén, Y. Yatabe
Study supervision: L. Fernandez-Cuesta, Y. Yatabe, R.K. Thomas
Biobanking of tumor samples: D. Moro-Sibilot
Cell culture work, molecular biological work (e.g., PCR): M. Koker, A. la Torre
Histological review: E. Brambilla, Y. Yatabe
Laboratory work: I. Dahmen
Sample contribution: L.A. Muscarella, A. la Torre

Acknowledgments

The authors are indebted to the patients who donated their tumor specimens as part of the Clinical Lung Cancer Genome

Published OnlineFirst January 27, 2014; DOI: 10.1158/2159-8290.CD-13-0633

Project initiative. Additional biospecimens for this study were obtained from the Victorian Cancer Biobank, Melbourne, Australia. The Institutional Review Board (IRB) of each participating institution approved collection and use of all patient specimens in this study. The authors thank Philipp Lorimier, Marek Franitza, Graziella Bosco, and Juan Luis Fernandez Mendez de la Vega for their technical assistance. The authors also thank the regional computing center of the University of Köln (RRZK) for providing the CPU time on the DFG-funded supercomputer "CHEOPS" as well as for the support.

Grant Support

This work was supported by the Deutsche Krebshilfe as part of the small-cell lung cancer genome-sequencing consortium (grant ID: 109679 to R.K. Thomas, M. Peifer, R. Buettner, S.A. Haas, and M. Vingron); by the EU-Framework Programme CURELUNG (HEALTH-F2-2010-258677 to E. Brambilla, J. Wolf, and R.K. Thomas); by the Deutsche Forschungsgemeinschaft through TH1386/3-1 (to R.K. Thomas); and through SFB832 (TP5 to L.C. Heukamp; and TP6 to R.T. Ullrich, J. Wolf, and R.K. Thomas); by the German Ministry of Science and Education (BMBF) as part of the NGFNplus program (grant 01GS08101 to J. Wolf and R.K. Thomas); by the Deutsche Krebshilfe as part of the *Oncology Centers of Excellence* funding program (to R. Buettner, J. Wolf, and R.K. Thomas); by a Stand Up To Cancer Innovative Research Grant, a Program of the Entertainment Industry Foundation (SU2C-AACR-IRG60109 to R.K. Thomas); by funds of the DFG Excellence Cluster ImmunoSensation (to J. Daßler); by the Italian Ministry of Health (Ricerca Corrente RC1303LO57 and GR Program 2010-2316264) and by the "5 × 1000" voluntary contributions (to L.A. Muscarella); by the Project for Development of Innovative Research on Cancer Therapeutics (P-Direct), Ministry of Education, Culture, Sports, Science and Technology of Japan (to Y. Yatabe); by a research project grant (IWT 110431 to D. Brehmer); by the Belgium government agency for Innovation by Science and Technology (IWT; to I. Lahortiga, S. Ogata, M. Parade, T. Perera, and D. Brehmer); and by Agiradom and French Health Ministry (PPHRC; to C.G. Brambilla).

Received September 13, 2013; revised January 21, 2014; accepted January 23, 2014; published OnlineFirst January 27, 2014.

REFERENCES

1. Pao W, Hutchinson KE. Chipping away at the lung cancer genome. Nat Med 2012;18:349–51.
2. Soda M, Choi YL, Enomoto M, Takada S, Yamashita Y, Ishikawa S, et al. Identification of the transforming *EML4-ALK* fusion gene in non-small-cell lung cancer. Nature 2007;448:561–6.
3. Takeuchi K, Soda M, Togashi Y, Suzuki R, Sakata S, Hatano S, et al. *RET, ROS1* and *ALK* fusions in lung cancer. Nat Med 2012;18:378–81.
4. Kohno T, Ichikawa H, Totoki Y, Yasuda K, Hiramoto M, Nammo T, et al. *KIF5B-RET* fusions in lung adenocarcinoma. Nat Med 2012;18:375–7.
5. Lipson D, Capelletti M, Yelensky R, Otto G, Parker A, Jarosz M, et al. Identification of new *ALK* and *RET* gene fusions from colorectal and lung cancer biopsies. Nat Med 2012;18:382–4.
6. Chao BH, Briesewitz R, Villalona-Calero MA. *RET* fusion genes in non-small-cell lung cancer. J Clin Oncol 2012;30:4439–41.
7. Ohashi K, Maruvka YE, Michor F, Pao W. Epidermal growth factor receptor tyrosine kinase inhibitor-resistant disease. J Clin Oncol 2013;31:1070–80.
8. Camidge DR, Bang Y-J, Kwak EL, Iafrate AJ, Varella-Garcia M, Fox SB, et al. Activity and safety of crizotinib in patients with *ALK*-positive non-small-cell lung cancer: updated results from a phase 1 study. Lancet Oncol 2012;2045:11–5.
9. Bergethon K, Shaw AT, Ou S-H, Katayama R, Lovly CM, McDonald NT, et al. *ROS1* rearrangements define a unique molecular class of lung cancers. J Clin Oncol 2012;30:863–70.
10. Shaw AT, Kim D-W, Nakagawa K, Seto T, Crinó L, Ahn M-J, et al. Crizotinib versus chemotherapy in advanced *ALK*-positive lung cancer. New Engl J Med 2013;368:2385–94.
11. Hynes NE, Lane HA. ERBB receptors and cancer: the complexity of targeted inhibitors. Nat Rev Cancer 2005;5:341–54.
12. Mei L, Xiong W. Neuregulin 1 in neural development, synaptic plasticity and schizophrenia. Nat Rev Neurosci 2008;9:437–52.
13. Talmage DA. Mechanisms of neuregulin action. Novartis Found Symp 2008;289:74–84.
14. Maeda Y, Tsuchiya T, Hao H, Tompkins DH, Xu Y, Mucenski ML, et al. $KRAS^{G12D}$ and NKX2-1 haploinsufficiency induce mucinous adenocarcinoma of the lung. J Clin Invest 2012;122:4388–400.
15. Falls D. Neuregulins: functions, forms, and signaling strategies. Exp Cell Res 2003;284:14–30.
16. Wallasch C, Weiss FU, Niederfellner G, Jallal B, Issing W, Ullrich A. Heregulin-dependent regulation of HER2/neu oncogenic signaling by heterodimerization with HER3. EMBO J 1995;14:4267–75.
17. Imielinski M, Berger AH, Hammerman PS, Hernandez B, Pugh TJ, Hodis E, et al. Mapping the hallmarks of lung adenocarcinoma with massively parallel sequencing. Cell 2012;150:1107–20.
18. The Clinical Lung Cancer Genome Project (CLCGP), Network Genomic Medicine (NGM). A genomics-based classification of human lung tumors. Sci Transl Med 2013;5:209ra153.
19. Yarden Y, Pines G. The ERBB network: at last, cancer therapy meets systems biology. Nat Rev Cancer 2012;12:553–63.
20. Peifer M, Fernández-Cuesta L, Sos ML, George J, Seidel D, Kasper LH, et al. Integrative genome analyses identify key somatic driver mutations of small-cell lung cancer. Nat Genet 2012;44:1104–10.
21. Wilbertz T, Wagner P, Petersen K, Stiedl A-C, Scheble VJ, Maier S, et al. *SOX2* gene amplification and protein overexpression are associated with better outcome in squamous cell lung cancer. Mod Pathol 2011;24:944–53.

Quantitative Proteomic Profiling Identifies DPYSL3 as Pancreatic Ductal Adenocarcinoma-Associated Molecule That Regulates Cell Adhesion and Migration by Stabilization of Focal Adhesion Complex

Takeo Kawahara[1,3], Naoe Hotta[1], Yukiko Ozawa[1], Seiichi Kato[1,4], Keiko Kano[1], Yukihiro Yokoyama[3], Masato Nagino[3], Takashi Takahashi[1], Kiyoshi Yanagisawa[1,2*]

1 Division of Molecular Carcinogenesis, Nagoya University Graduate School of Medicine, Nagoya, Aichi, Japan, **2** Institute for Advanced Research, Nagoya University, Nagoya, Aichi, Japan, **3** Division of Surgical Oncology, Nagoya University Hospital, Nagoya, Aichi, Japan, **4** Department of Pathology and Molecular Diagnostics, Nagoya University Hospital, Nagoya, Aichi, Japan

Abstract

Elucidation of how pancreatic cancer cells give rise to distant metastasis is urgently needed in order to provide not only a better understanding of the underlying molecular mechanisms, but also to identify novel targets for greatly improved molecular diagnosis and therapeutic intervention. We employed combined proteomic technologies including mass spectrometry and isobaric tags for relative and absolute quantification peptide tagging to analyze protein profiles of surgically resected human pancreatic ductal adenocarcinoma tissues. We identified a protein, dihydropyrimidinase-like 3, as highly expressed in human pancreatic ductal adenocarcinoma tissues as well as pancreatic cancer cell lines. Characterization of the roles of dihydropyrimidinase-like 3 in relation to cancer cell adhesion and migration *in vitro*, and metastasis *in vivo* was performed using a series of functional analyses, including those employing multiple reaction monitoring proteomic analysis. Furthermore, dihydropyrimidinase-like 3 was found to interact with Ezrin, which has important roles in cell adhesion, motility, and invasion, while that interaction promoted stabilization of an adhesion complex consisting of Ezrin, c-Src, focal adhesion kinase, and Talin1. We also found that exogenous expression of dihydropyrimidinase-like 3 induced activating phosphorylation of Ezrin and c-Src, leading to up-regulation of the signaling pathway. Taken together, the present results indicate successful application of combined proteomic approaches to identify a novel key player, dihydropyrimidinase-like 3, in pancreatic ductal adenocarcinoma tumorigenesis, which may serve as an important biomarker and/or drug target to improve therapeutic strategies.

Citation: Kawahara T, Hotta N, Ozawa Y, Kato S, Kano K, et al. (2013) Quantitative Proteomic Profiling Identifies DPYSL3 as Pancreatic Ductal Adenocarcinoma-Associated Molecule That Regulates Cell Adhesion and Migration by Stabilization of Focal Adhesion Complex. PLoS ONE 8(12): e79654. doi:10.1371/journal.pone.0079654

Editor: Martin Fernandez-Zapico, Schulze Center for Novel Therapeutics, Mayo Clinic, United States of America

Received July 2, 2013; **Accepted** October 3, 2013; **Published** December 5, 2013

Funding: This work was supported in part by Exploratory Research and Program for Improvement of Research Environment for Young Researchers from Special Coordination Funds for Promoting Science and Technology commissioned from the Ministry of Education, Culture, Sports, Science and Technology of Japan; and Grants-in-Aid for Scientific Research (C) from the Japan Society for the Promotion of Science; and Grant-in-Aid for the Third Term Comprehensive Control Research for Cancer commissioned from Ministry of Health, Labor and Welfare. The funders had no role in study design, data collection and analysis, decision to publish, or preparation of the manuscript.

Competing interests: The authors have declared that no competing interests exist.

* E-mail: kyana@med.nagoya-u.ac.jp

Introduction

Pancreatic cancer is the fifth leading cause of cancer death in Japan with more than 24,000 annual deaths [1], while lung cancer is another hard-to-cure cancer with the highest death tolls of more than 70,000 lives a year [2]. Widespread metastasis and/or massive local invasion are commonly present, when they are diagnosed, making long-term survival of these cancers remain unsatisfactory. Thus, it is evident that elucidation of the underlying mechanisms of invasion and distant metastasis is crucial to improve the current dismal outcome. Along this line, we previously established a highly metastatic clone (NCI-H460-LNM35, hereafter referred to as LNM35) of a non-small cell lung cancer cell line, which helped to identify involvement of the *COX-2*, *CLCP-1*, and *DLX-4* genes in cancer metastasis through global expression profiling analysis of LNM35 and its low-metastatic parental clone, NCI-H460-N15 (herein called N15) [3–8].

Comprehensive analysis of protein expression patterns in biological materials may improve understanding of the molecular complexities of human diseases, and could be useful to detect diagnostic or predictive protein expression patterns that reflect clinical features. We previously employed Matrix-assisted laser desorption/ionization mass spectrometry (MALDI MS) for expression profiling of proteins in human lung cancer specimens and found that the resultant proteomic patterns could predict various clinical features [9,10]. We have employed quantitative proteomic analysis with the use of a peptide tagging technology, isobaric tags for relative and absolute quantification (iTRAQ), in order to obtain mechanistic insight into metastasis in human lung cancer [11]. However, only limited number of studies in the area of pancreatic cancer research have exploited this high-throughput method, and various proteins thus far identified as differentially expressed during the development of pancreatic cancer have not been studied in detail in order to gain molecular insight into the aggressive nature of this devastating cancer with frequent massive invasion and distant metastasis [12,13].

In the present study, we searched for proteins differentially expressed between cancerous and normal pancreatic duct epithelium through proteomic profiling with iTRAQ, which resulted in the identification of high expression of dihydropyrimidinase-like 3 (DPYSL3) in human pancreatic cancer. We also report detailed functional characterizations of DPYSL3 in relation to cancer cell proliferation, invasion, and metastasis by applying a combined proteomic approach with the aid of multiple reaction monitoring (MRM) technology.

Results

Identification of differentially expressed DPYSL3 in pancreatic ductal adenocarcinoma

We compared the protein profiles between a set of 7 individual fresh-frozen pancreatic ductal adenocarcinoma (PDAC) specimens and a mixture of 3 pooled normal main pancreatic duct (MPD) tissue specimens using mass spectrometry combined with iTRAQ peptide tagging technology, and identified 1015 proteins (Figure 1A and Table S3). For each patient, we selected proteins based on the relative expression in PDAC tissue as compared with pooled MPD that was greater than the average ratio +2 SD, then evaluated the frequency of the selected proteins in the 7 PDAC patients. Accordingly, we found 19 up-regulated proteins that were selected in at least 2 specimens (Table 1). Among those, up-regulation of dihydropyrimidinase-related protein 3 (DPYSL3), histone H2B type 1-J (H2BJ), and glutathione S-transferase P1 (GSTP1) was observed in all 7 of the PDAC specimens (Figure 1B). Up-regulation of H2BJ and GSTP1 is considered to reflect a higher rate of PDAC cell division [15,16] . However, the functional relationship between the characteristics of PDAC and dihydropyrimidinase is unclear. Accordingly, we initially employed western blotting to verify the proteomic data using an independent validation set of PDAC tissue specimens. Expression of DPYSL3 protein was observed in 16 of 22 (77.7%) PDAC tissues, whereas signal of DPYSL3 was not confirmed in the 3 MPD specimens that comprised an independent validation cohort in western blotting (Figure 2 and Table S2). Since mass spectrometric analyses sometimes show higher sensitivity than western blot analyses depending upon specificity and sensitivity of antibody used, though the signal from DPYSL3 were confirmed in 3 pooled MPD in MS profiling, we could not detect it in all of 3 MPD specimens that comprised an independent validation cohort in western blot analyses. Of note, three additional bands other than wild-type DPYSL3 were observed in western blotting analyses, thus we investigated the possibility that these bands reflected modification of DPYSL3. DPYSL3-positive PDAC cell lines (Figure 3A and Figure S1A) were treated with phosphatase and a glycosylation inhibitor and subjected to western blotting assay, however, no significant change was observed (Figure S1B). Since we confirmed DPYSL3 expression in SU86.86 cells, which expresses one of additional products, using MRM analyses with 6 different transitions (Figure 3B and Figure S2), we understand that heterogeneous bands observed in this cell line as well as PDAC tissue specimens may be alternative splicing variants of DPYSL3. We next employed Image J software to compare expression level of DPYSL3 across PDAC patients, and divided them into two groups, high-DPYSL3 and low-DPYSL3, according to DPYSL3/β-actin ratio (Table S2). We conducted statistical analyses to evaluate the significance of DPYSL3 expression in relation to the listed clinical characteristics, however, no significant association between DPYSL3 and clinical characteristics was observed.

Involvement of DPYSL3 in pancreatic cancer cell survival

Next, we examined whether DPYSL3 knockdown affects the viability of pancreatic cancer cells. Since CFPAC-1 cells were shown to highly express DPYSL3 protein and mRNA in western blotting analysis and real-time RT-PCR, respectively, as compared with immortalized normal pancreatic duct cells (ACBRI515) (Figure 3A and Figure S1A), siDPYSL3 was introduced into CFPAC-1 cells and an MTT assay was employed to evaluate the effect of DPYSL3 knockdown. As shown in Figure 3C, cell viability was significantly reduced by addition of siDPYSL3 into DPYSL3-positive CFPAC-1 cells, whereas the DPYSL3-negative MIA PaCa2 and PANC-1 pancreatic cancer cell lines did not show any such effect (Figure S3). Introduction of 2 different siRNAs against DPYSL3 (#1 and #2) showed similar inhibitory effects on cell proliferation, demonstrating the specificity of siRNA-mediated DPYSL3 knockdown (Figure 3C). Flow-cytometric analysis revealed an increase in the sub-G1 population of CFPAC-1 cells after introduction of siDPYSL3, suggesting that the induction of apoptosis is part of the mechanism for reduction of cell viability (Figure 3D). Accordingly, we investigated expressions of cleaved-PARP and -caspase-8 in siDPYSL3-treated CFPAC-1 cells, and found that slight induction of these cleaved products in siDPYSL3-treated adhering cells (Figure 3E). Since siDPYSL3-treated CFPAC-1 cells showed a rounded morphology and many of the cells were detached from the bottom of the culture dishes (Figure S4), we speculated that DPYSL3-knockdown cells die after detachment. To